

2009

## FIBRONECTIN CONJUGATION ONTO THREE-DIMENSIONAL POROUS POLYURETHANE SCAFFOLDS FOR VASCULAR TISSUE ENGINEERING

Gaytri Dubey

Follow this and additional works at: <https://ir.lib.uwo.ca/digitizedtheses>

---

### Recommended Citation

Dubey, Gaytri, "FIBRONECTIN CONJUGATION ONTO THREE-DIMENSIONAL POROUS POLYURETHANE SCAFFOLDS FOR VASCULAR TISSUE ENGINEERING" (2009). *Digitized Theses*. 4078.  
<https://ir.lib.uwo.ca/digitizedtheses/4078>

This Thesis is brought to you for free and open access by the Digitized Special Collections at Scholarship@Western. It has been accepted for inclusion in Digitized Theses by an authorized administrator of Scholarship@Western. For more information, please contact [wlsadmin@uwo.ca](mailto:wlsadmin@uwo.ca).

**FIBRONECTIN CONJUGATION ONTO THREE-DIMENSIONAL  
POROUS POLYURETHANE SCAFFOLDS FOR VASCULAR  
TISSUE ENGINEERING**

(Spine title: Fibronectin Conjugation onto 3D PCU Scaffolds)

(Thesis format: Monograph)

by

**Gaytri Dubey**

Graduate Program in Engineering Science  
Department of Chemical and Biochemical Engineering

Submitted in partial fulfillment  
of the requirements for the degree of  
Master of Engineering Science

School of Graduate and Postdoctoral Studies  
The University of Western Ontario  
London, Ontario

© Gaytri Dubey 2009

## Abstract

In tissue engineering, scaffolds serve as the three-dimensional (3D) structural framework controlling cell behavior and ultimately the performance of the final construct. Cell interactions with synthetic scaffolds can be improved by attaching biomolecules such as proteins or peptides. Fibronectin (FN) is a protein that contains several domains including the cell adhesion tri-peptide, Arginine-Glycine-Aspartic Acid, allowing it to mediate cell attachment and proliferation on various substrates. In this work, FN was conjugated on 3D highly porous poly(carbonate) urethane (PCU) scaffolds through grafted poly(acrylic) acid (AA) spacers. Scaffolds were fabricated using a solvent casting-particulate leaching method. AA was grafted on the 3D scaffolds using a ceric ion initiator, and FN was conjugated using an N-hydroxysuccinimide intermediate. Scaffold pore structures were visualized using scanning electron microscopy and Fourier transform infrared spectroscopy was used to monitor reaction progress. A toluidine blue assay was used to quantify grafted AA groups. Survey and high-resolution X-ray photoelectron spectroscopy scans of scaffolds provided changes in atomic composition and chemical groups, respectively. Immunofluorescence studies showed FN to be evenly distributed over the scaffold surface.

**Keywords:** Biomaterials, Fibronectin, Polyurethane, Three-Dimensional Scaffolds, Tissue Engineering, Vascular Smooth Muscle Cells.

## **Acknowledgements**

I would like to express my gratitude towards my supervisor, Dr. Kibret Mequanint, for his guidance and advice during my study at The University of Western Ontario. I would also like to thank my lab group for their encouragement, and Dr. Shigang Lin for his help with the cell studies. I wish to acknowledge the Natural Sciences and Engineering Research Council of Canada (NSERC) for providing me with financial support to conduct my research. Dr. Mark Biesinger deserves mention for conducting the XPS work at Surface Science Western. Last but not least, I wish to thank my family for their ongoing support and encouragement.

## Table of Contents

Certificate of Examination .....	ii
Abstract .....	iii
Acknowledgements .....	iv
Table of Contents .....	v
List of Tables .....	vii
List of Figures .....	viii
List of Abbreviations .....	x
CHAPTER 1 .....	1
1 Introduction .....	1
1.1 Tissue Engineering .....	1
1.2 Strategies of Tissue Engineering .....	1
1.2.1. Clinical Need for Vascular Tissue Engineering .....	4
1.3 Scaffolds in Tissue Engineering .....	12
1.3.1. Scaffolds from Natural Materials .....	13
1.3.2. Synthetic Scaffold Materials .....	14
1.3.3. Biomimetic Scaffolds .....	15
1.3.3.1. Fibronectin and RGD .....	15
1.4 Techniques in Scaffold Fabrication .....	18
1.5 Immobilization Strategies of FN onto 3D Scaffolds .....	22
1.6 Objectives and Rationale .....	27
CHAPTER 2 .....	29
2 Materials and Methods .....	29
2.1 Materials .....	29
2.2 Scaffold Fabrication .....	30
2.3 Acrylic Acid Grafting onto Porous 3D Polyurethane Scaffolds .....	32
2.4 Fibronectin Conjugation .....	32
2.5 Scaffold Characterization .....	34
2.5.1. Scanning Electron Microscopy (SEM) .....	34
2.5.2. Fourier Transform-Infrared Microscopy (FT-IR) .....	34
2.5.3. Toluidine Blue (TB) Assay .....	34

2.5.4.	X-Ray Photoelectron Spectroscopy (XPS) .....	35
2.5.5.	Immunofluorescence Microscopy .....	35
2.5.6.	Bicinchoninic Acid (BCA) Assay .....	36
2.6	Cell Work .....	37
CHAPTER 3	.....	38
3	Results .....	38
3.1	Chemistry and FT-IR Analysis .....	38
3.2	Toluidine Blue Assay .....	45
3.2.1.	Effect of Time on the Moles of COOH Grafted .....	46
3.2.2.	Effect of Acrylic Acid Concentration on the Moles of COOH Grafted .....	49
3.3	XPS Study of FN Conjugation to Scaffolds .....	50
3.3.1.	Survey Scans on Scaffolds .....	50
3.3.2.	High Resolution XPS Scans on Scaffolds .....	57
3.4	SEM Observation of Scaffolds .....	64
3.5	FN Leaching Study Using the BCA Assay .....	66
3.6	Immunofluorescence Study of FN on Various Scaffolds .....	69
3.7	Preliminary Cell Culture Studies .....	71
CHAPTER 4	.....	76
4	Conclusions .....	76
4.1	Summary .....	76
4.2	Future Directions .....	77
References	.....	78
Appendix A: Tabulated XPS Survey Scan Data	.....	87
Curriculum Vitae	.....	88

## List of Tables

Table 1. Fibronectin-binding integrins and the key recognition site in fibronectin for binding. . . . .	16
Table 2. The atomic composition of PCU, PCU-AA, and PCU-AA-FN scaffolds as determined by XPS survey scans for 1 h, 6 M AA grafts. ....	49
Table 3. The atomic composition of PCU, PCU-AA, and PCU-AA-FN scaffolds as determined by XPS survey scans for 6 h, 6 M AA grafts. ....	54
Table 4. High resolution XPS C1s scan results for PCU, PCU-AA, and PCU-AA-FN scaffolds. Values represent the percent associated to each bond type. ....	57
Table 5. High resolution XPS N1s and O1s scan results for PCU, PCU-AA, and PCU-AA-FN scaffolds. Values represent the percent associated to each bond type. ....	57

## List of Figures

Figure 1. Schematic of the solvent-casting particulate leaching scaffold fabrication method.....	20
Figure 2. Chemical structure of Bionate 80A, the polycarbonate urethane used in this work. ....	30
Figure 3. Schematic drawing of the pressure differential scaffold casting apparatus.....	31
Figure 4. FN conjugation scheme onto 3D porous PCU scaffolds.....	33
Figure 5. Chemical structure of toluidine blue. ....	35
Figure 6. FT-IR spectra of: (A) PCU; (B) PCU-AA; (C) PCU-AA-NHS; (D) PCU-AA-FN scaffolds.....	40
Figure 7. Expanded view of the 1800-1000 $\text{cm}^{-1}$ region for (A) PCU; (B) PCU-AA; (C) PCU-AA-NHS; and (D) PCU-AA-FN scaffolds. ....	41
Figure 8. Expanded view of FT-IR spectra for PCU-AA-FN scaffolds in the characteristic amide I, II, and III regions. ....	42
Figure 9. A calibration curve correlating the absorbance read by a UV-Vis spectrometer at 633 nm and the concentration of toluidine blue in solution.....	44
Figure 10. The effect of grafting time on the amount of COOH groups incorporated into the PCU scaffolds at a fixed concentration of 6 M acrylic acid. ....	45
Figure 11. The rate of moles of AA consumed in the grafting reaction as a function of time at 6M AA concentration. ....	47
Figure 12. The effect AA concentration on the amount of COOH groups grafted onto PCU scaffolds for a fixed reaction time of 1 h. ....	48
Figure 13. XPS analysis of N1s levels for PCU, PCU-AA, PCU-AA-NHS and PCU-AA-FN scaffolds.....	50
Figure 14. XPS analysis on N <sub>1s</sub> and S <sub>2p</sub> for FN immobilized scaffolds on 1 h 6 M AA grafts for 24 h.....	52
Figure 15. XPS analysis on the effect of FN conjugation time on the atomic % N <sub>1s</sub> and S <sub>2p</sub> using 0.5 mg FN.....	53

Figure 16. XPS analysis on N <sub>1s</sub> and S <sub>2p</sub> for FN immobilized on 6 h 6M AA grafts. ....	55
Figure 17. High resolution XPS N <sub>1s</sub> spectra of PCU, PCU-AA, and PCU-AA-FN scaffolds showing peak integrations. ....	59
Figure 18. High resolution XPS C <sub>1s</sub> spectra of PCU, PCU-AA, and PCU-AA-FN scaffolds showing peak integrations. ....	61
Figure 19. High resolution XPS O <sub>1s</sub> spectra of PCU, PCU-AA, and PCU-AA-FN scaffolds showing peak integrations. ....	62
Figure 20. Scanning electron micrographs of PCU scaffolds. ....	64
Figure 21. A calibration curve for the BCA assay correlating the concentration of FN in solution with the absorbance read at 562 nm with a UV-Vis spectrophotometer. ....	66
Figure 22. Quantities of FN leached with time from PCU-AA-FN (0.5 mg FN) and PCU-AA FN adsorbed (0.5 mg FN) scaffolds. ....	67
Figure 23. Immunofluorescence results for various PCU-AA-FN scaffolds. ....	69
Figure 24. Fluorescent microscope images of vascular smooth muscle cell behavior on (A) PCU; (B) PCU-AA; (C) PCU-AA FN adsorbed (0.5 mg FN); (D) PCU-AA-FN (0.5 mg FN) after 4 days of culture. ....	71
Figure 25. Confocal microscope images of VSMC interaction with PCU-AA FN adsorbed (0.5 mg FN) (A-B); PCU-AA-FN (0.5 mg FN) (C-D); PCU-AA-FN (0.5 mg FN) exposed to 2% SDS (E-F), after 4 days culture. ....	73

## List of Abbreviations

AA	Acrylic Acid
BCA	Bicinchoninic acid assay
DMF	N,N-dimethylformamide
ECM	Extracellular matrix
EDC	1-Ethyl-3-(3-dimethylaminopropyl) carbodiimide hydrochloride
EPC	Endothelial progenitor cells
FN	Fibronectin
FTIR	Fourier transform infrared spectroscopy
LDV	Leucine-Aspartic acid-Valine
MES	4-Morpholineethanesulfonic acid
NHS	N-hydroxysuccinimide
PBS	Phosphate buffered saline
PCU	Polycarbonate urethane
PHSRN	Proline-Histidine-Serine-Arginine-Asparagine
PFA	Paraformaldehyde
PGA	Poly(glycolic) acid
PLA	Poly(lactic) acid
PLLA	Poly(L-lactide) acid
PTFE	Polytetrafluoroethylene
REDV	Arginine-Glutamic Acid-Aspartic acid-Valine
RGD	Arginine-Glycine-Aspartic acid

SEM	Scanning electron microscopy
SDS	Sodium dodecyl sulfate
TB	Toluidine blue
XPS	X-ray photoelectron spectroscopy
YIGSR	Tyrosine-Isoleucine-Glycine-Serine-Arginine

# CHAPTER 1

## **1 Introduction**

### **1.1 Tissue Engineering**

**T**issue engineering is an interdisciplinary field that applies principles and methods of engineering and the life sciences toward the development of biological substitutes that restore, maintain, and improve the function of damaged tissues and organs<sup>1</sup>. The broad term “tissue engineering” describes a set of tools interfacing the biomedical engineering sciences, allowing living and endogenous cells to aid tissue formation or regeneration for a therapeutic benefit, either to restore, maintain, or enhance tissues and organs<sup>2,3</sup>. Besides the obvious therapeutic applications, tissue engineering can also be extended to diagnostics for *in vitro* testing of drug metabolism, uptake, toxicity, and pathogenicity<sup>4</sup>.

### **1.2 Strategies of Tissue Engineering**

Generally, there are four main tissue engineering strategies: cell transplantation, scaffold implantation, cell-seeded scaffold implantation, and *in vitro* tissue engineering<sup>2</sup>. In the cell transplantation strategy, cells are directly injected into a region of damaged tissue where they are needed. For instance, the injection of cardiac muscle cells into the heart

tissue and injection of dopaminergic cells into the brain to replace cells lost during Parkinson's disease fall into this category. The encapsulation and transplantation of allogenic pancreatic beta cells for the treatment type I diabetes is a conceptually simple and appealing cell transplantation strategy<sup>5,6</sup>. There have also been investigations in hepatocyte transplantation for treatment of acute liver failure<sup>7</sup>. In myocardial tissue engineering, myocytic cells have been injected in the vicinity of a damaged myocardium<sup>8</sup>. Thus the transplantation of murine atrial tumor cells, neonatal porcine myocytes, and human fetal cardiomyocytes into the left ventricular wall of adult swine showed no significant rejection and, cells appeared to thrive and form close association with host myocytes<sup>9</sup>. Unfortunately, injection of cells into a tissue site does not guarantee the formation of a functional tissue. In this regard, the limitations to cell transplantation strategy include immune rejection, loss of specific cellular function, and poor integration with host cells.

The scaffold implantation strategy involves the implantation of a scaffold into a host to recruit endogenous cells to repopulate and remodel the scaffold. The implantation of decellularized heart valves and synthetic vascular grafts in order to repopulate and remodel the tissue while preserving architectural and chemical information is a common practice<sup>2</sup>. Although there have been failures in the past, scaffold implantation to repair damaged or diseased tissues is an active area of clinical practices and research innovation. As this technique relies on native cells migrating and populating a graft, one of the key challenges is poor cell recruitment and maintenance<sup>10</sup>.

The cell-seeded scaffold implantation strategy uses a scaffold seeded with cells that is implanted into the host without *in vitro* maturation. This strategy is used primarily in endothelial cell seeding. As an example, isolated endothelial progenitor cells (EPC) were expanded *ex vivo*, seeded on decellularized porcine iliac vessels, and grafted in the carotid position in sheep<sup>11</sup>. Results demonstrated that EPC-seeded grafts remained patent for 130 days, whereas non-seeded grafts occluded within 15 days. Poor cell attachment and cell seeding densities, however, limit the effectiveness of this technique.

In the most commonly used paradigm, *in vitro* tissue engineering involves seeding cells on a natural or synthetic scaffold and allowing the construct to mature *in vitro*, usually in a bioreactor. In this strategy seeded cells will infiltrate the scaffolds, proliferate and lay their own ECM while the scaffold may or may not be degraded. The matured tissue is then implanted into the host, where further remodeling occurs *in vivo*<sup>2</sup>.

There are three distinctive elements for *in vitro* tissue engineering: cells, scaffolds, and bioreactors. The sources for cells used for tissue engineering purposes can be autologous (host), homologous (same species), or heterologous (cross-species)<sup>12</sup>. Ideally, isolated cells should be easily accessible, be multipotent to differentiate into a variety of organ-specific cells with specialized function, be highly proliferative *in vitro* without being mutagenic *in vivo*, and be compatible with the recipient's immune system. Cell types such as fibroblasts, hepatocytes and endothelial cells proliferate rapidly *in vitro* whereas other cell types such as neural cells, smooth muscle cells, or adult cardiomyocytes, proliferate slowly or not at all<sup>13</sup>. Intuitively, one of the main challenges in the tissue

engineering process is the need for a suitable supporting scaffold for the control of cell behavior and organization, and this is the main topic of this research that will be described in detail in Section 1.3.

### **1.2.1. Clinical Need for Vascular Tissue Engineering**

The prevalence of cardiovascular disease (CVD) and subsequent mortality rates is a serious health threat in North America<sup>14</sup>. Statistically, CVD is the leading cause of death and the leading economic burden of disease in Canada<sup>15</sup>. Coronary artery disease is the most prevalent form of heart disease<sup>14</sup>. Despite advances made in balloon angioplasty as a minimally invasive surgery, surgical intervention to replace or bypass a damaged or otherwise diseased vessel is one of the routine clinical procedures performed<sup>16</sup>. Common vascular graft material choices are the saphenous vein and mammary artery. The saphenous vein may have varicose degenerative changes that can lead to the formation of an aneurysm when transplanted to a high-pressure arterial site<sup>17</sup> and although the mammary artery seldom develops atherosclerosis, it may not be of appropriate dimensions. Furthermore, many patients do not have the appropriate blood vessels to use as a replacement either due to diseased blood vessels or because the blood vessel was already used in a previous surgery<sup>18</sup>. The other choice is xenogeneic vascular substitutes but such tissues have drawbacks due to potential inter-species disease transmission and immunological rejection.

In the absence of a suitable vascular substitute from the aforementioned choices, current therapy involves the surgical replacement of diseased vessels with prosthetic devices or

grafts, although limitations and serious complications have been reported in these procedures<sup>16-19</sup>. Clinically used synthetic grafts constructed from Dacron® (polyethylene terephthalate; PET) or Teflon® (expanded polytetrafluoroethylene; ePTFE) are satisfactory for large diameter vascular replacement where the blood flow rate is high and the resistance is low<sup>19</sup>. These grafts, however, fail miserably when used for small diameter vessel replacement (6 mm internal diameter and below) due to blood coagulation on the luminal surface<sup>17,18</sup>.

Vascular tissue engineering serves as a promising approach to current treatment modalities of diseased blood vessels. Tissue engineered blood vessels (TEBV) are functional and viable, having the ability to grow, repair, and remodel with time. As an advantage over synthetic grafts, they are designed to be non-thrombogenic and responsive both mechanically and biologically to hemodynamic stresses experienced *in vivo*. Although vascular tissue engineering has progressed considerably with nearly 25 years of expertise in the field, it is still at the early stages. There are many hurdles that need to be overcome before tissue engineered blood vessel replacements are available for humans. Adequate mechanical strength and elasticity in a hemodynamic cyclic loading environment, non-thrombogenicity, resistance to infection, and control of cell function are several challenges that are under investigation. For example, native arteries have circumferential wall stresses of at least 6 MPa and rupture strengths greater than 2000 mmHg<sup>20</sup>, and collagen-based vessel grafts thus far have wall stresses of 40-250 kPa and rupture strengths below 500 mmHg<sup>21</sup>. The engineered vessel should induce an acceptable healing response that does not result in inflammation, hyperplasia, or fibrous

capsule formation, and, ideally, the grafted vessel should integrate smoothly with the native tissue<sup>16</sup>. Although *in vivo* remodeling of the tissue is expected with time, tissue engineered vascular grafts must be functional immediately upon implantation<sup>18</sup>. From a surgical standpoint, ease of handling and suture retention are equally important criteria for engineered blood vessels.

#### **1.2.1.1. Properties of Blood Vessels**

It is necessary to understand the physiology of a blood vessel in order to engineer a functional artery *in vitro*. Blood vessels are comprised of three concentric layers. The innermost layer closest to blood flow is termed the tunica intima; it is composed of a non-thrombogenic monolayer of endothelial cells attached to a connective tissue bed of basement membrane and matrix molecules<sup>22</sup>. These endothelial cells secrete molecules such as nitric oxide (NO) in order to inhibit platelet activation and prevent thrombus formation<sup>23</sup>. The tunica media is the middle layer, and is comprised of densely populated smooth muscle cells organized concentrically, with bands or fibers of elastic tissue<sup>18</sup>. It is separated from the intima layer by elastic lamina. The outermost layer, the tunica adventitia, is composed of a collagenous extracellular matrix and fibroblast cells and functions to add rigidity.

The mechanical properties critical to blood vessel function include the tensile stiffness, elasticity, and viscoelasticity. The complex extracellular matrix (ECM) surrounding the vascular cells imparts the biomechanical properties of the tissue. This ECM consists of collagen (types I and III), elastin fibers, proteoglycans (versican, decorin and biglycan,

lumican and perlecan, hyaluronan) and glycoproteins (laminin, fibronectin, thrombospondin and tenascin)<sup>18</sup>. The collagens provide the tensile stiffness at high mechanical strains, elastin dictates tissue mechanics at low strains and confers elastic stretch and recoil, proteoglycans contribute to compressibility, and in combination with collagen and elastin they are responsible for the anisotropy properties<sup>18,23</sup>.

### **1.2.1.2. Tissue Engineering Blood Vessels – A Historical Perspective**

In 1986, Weinberg and Bell were the first to design and engineer blood vessels using a collagen scaffold seeded with bovine aortic endothelial cells, smooth muscle cells, and adventitial fibroblasts<sup>24</sup>. The cells were shown to be healthy and functional in the construct, and the strength of the construct was dependent upon the layered integration of collagen with a Dacron mesh. Despite this early success, the construct failed to meet the mechanical load of the *in vivo* hemodynamic environment as well as the burst strength of native arteries.

Since Weinberg and Bell, there have been advances in constructing tissue engineered blood vessels (TEBVs). The survey presented here is not an exhaustive list, but highlights interesting attempts in the field. Hirai et al. fabricated vascular constructs from type I collagen and bovine aortic smooth muscle cells (SMCs). Thus a hybrid medial tissue was prepared by pouring a cold solution of SMCs and type I collagen into a tubular glass mold composed of a mandrel and a sheath<sup>25</sup>. Upon incubation at 37°C, the SMCs incorporated the collagen gel, and subsequently the sheath was removed. Seeding of cells

at a higher density and a lower concentration of collagen resulted in rapid and prominent shrinkage<sup>25</sup>. The final tissues only withstood luminal pressures of 100 mmHg.

L'Heureux et al. used a novel strategy in designing tissue engineered blood vessels (TEBVs) without using scaffolds<sup>22</sup>. An acellular inner membrane (IM) was designed by dehydrating a tubular tissue of fibroblasts, and this was slipped around a tubular mandrel of PTFE. A sheet of SMCs was rolled around the IM, and after maturation in a bioreactor, a sheet of fibroblasts was wrapped around the SMC layer. The mandrel was removed after an 8 week period of maturation and the lumen was seeded with endothelial cells. The engineered vessel had burst strength exceeding 2000 mmHg, and was the first completely biological TEBV to display burst strength comparable to that of human vessels. Unfortunately, preliminary *in vivo* tests demonstrated a 50% patency rate and failures occurred within the first few days, as a result of occlusive thrombus formation.

A notable approach of artery design was established by Campbell et al. in 1999<sup>17</sup>. Silastic tubing of variable length and diameter was inserted into the peritoneal cavity of rats or rabbits. The resulting inflammatory response generated granulation tissue covered by a layer of mesothelium. Within 2 weeks, layers of myofibroblasts, collagen matrix, and a single layer of mesothelium covered the tubing. The significance of the mesothelium layer is its fibrinolytic and anticoagulant activity as synthetic grafts seeded with mesothelium are known to have a high patency rate similar to grafts seeded with endothelium<sup>17</sup>. The Silastic tubing was removed from the harvested implants and the tube of living tissue was inverted such that it now resembled a blood vessel with an inner

lining of nonthrombotic mesothelial cells (the “intima”), a media layer of smooth muscle–like cells (myofibroblasts), collagen, and elastin, and with an outer collagenous “adventitia.” The tissue was successfully grafted into the carotid artery or abdominal aorta of the same animal in which they were grown. The graft remained patent for at least 4 months and developed structures resembling elastic lamellae. Although the results were preliminary, some advantages of these grafts are their flexibility in sizing and design, non-thrombogenic surface, and importantly, absence of tissue rejection since they are grown inside the host’s body<sup>17</sup>.

Scaffold guided tissue engineering of vascular grafts was conducted by Niklason et al. (2001) whereby polyglycolic acid (PGA) scaffolds seeded with VSMCs were wrapped with a highly distensible silicon tubes and matured in a bioreactor<sup>26</sup>. A pulsatile pump operated at 165 beats per minute exerted systolic/diastolic pressures of 270/30 mmHg. The perfusion system provided a pulsatile flow of sterile PBS through the silicone tubing in the lumen of each engineered vessel. After 8 weeks of culture, the engineered vessels had the appearance of native vessels, and dynamic compliance of 5-week vessels was comparable to that of native arteries, although the burst strength of these vessels was substantially less than that of the native saphenous vein<sup>26</sup>.

In order to alleviate the problems associated with the mechanical properties of TEBVs, several groups have used non-degradable support sleeves, commonly Dacron<sup>®</sup>, to reinforce collagen-based constructs. Although these sleeves improve burst strengths to allow for *in vivo* implantation studies, they have a foreign material element. In 2002,

Berglund et al. created crosslinked type I collagen support sleeves<sup>27</sup>. Suspensions of human dermal fibroblasts in collagen were poured into tube molds containing tubular mandrel with inserted support sleeves. Once gelation had occurred, the mandrel was removed and the hybrid construct was cultured in dishes. Although the incorporation of sleeves significantly improved the mechanical properties of constructs (burst strength of 650 mmHg and peak tensile stresses to 350 kPa), they were still below those of native arteries. Furthermore, crack propagation of the glutaraldehyde crosslinked collagen sleeve led to abrupt construct failure.

The detailed review of historical approaches in TEBV is extensive and outside the scope of this thesis. Nonetheless, as exemplified by the aforementioned studies, there are substantial challenges faced in blood vessel tissue engineering. The lack of an elastic vessel that can withstand cyclic loading, compliance mismatch, and poor patency have continued to be a hindering factor to advances in tissue engineered blood vessel research.

### **1.2.1.3. Role of Vascular Smooth Muscle Cells**

Vascular smooth muscle cells (VSMCs) are derived from multiple embryonic origins including local mesenchymal, neural crest, and proepicardial cells<sup>28</sup>. In fetal development, VSMCs are responsible for the deposition of the medial layer of concentric rings of elastic lamellae, a major structural element of the arterial wall<sup>29</sup>. This type of VSMC behaviour is termed as the synthetic phenotype, where cells are involved in the morphogenesis of blood vessels, exhibiting high rates of proliferation, migration, and ECM protein production in order to develop the blood vessel wall while simultaneously acquiring contractile abilities<sup>30</sup>. One of the underlying reasons for TEBV mechanical

failures is due to the lack of adequate and mature elastic lamellae deposition by VSMCs<sup>23</sup>. Fully differentiated VSMCs have a low proliferation rate, synthesize small amounts of ECM proteins, and express a unique array of contractile proteins, ion channels, and signalling molecules required for their contractile phenotype function<sup>28,30</sup>. The primary function of VSMCs in mature blood vessels is contraction and regulation of blood vessel tone-diameter, blood pressure, and blood flow distribution<sup>30</sup>. In spite of this, fully differentiated VSMCs also demonstrate plasticity; they can undergo reversible phenotypic changes in response to environmental cues. In order to fabricate TEBV with sufficient elastin content, one must harness these cues to promote the synthetic phenotype in engineered vascular constructs. For example, it has been demonstrated that fibronectin promotes a phenotypic shift in isolated rat smooth muscle cells from a contractile to a synthetic phenotype within the first few days in primary culture<sup>31</sup>. Characteristic changes observed in cells grown on fibronectin coated plates included the loss of myofilaments, diminished ability to contract, and the extensive development of rough endoplasmic reticulum and a large golgi complex, which when stimulated result in cell proliferation and production of ECM components. *In vivo*, SMCs mainly experience cyclic tensile strains due to pressure forces of the blood and compression due to thinning of the vessel wall during inflation<sup>32</sup>. Mechanical and cyclic strain have been shown to increase the secretory function of VSMCs leading to increased ECM protein production, including the release of platelet derived growth factor (PDGF), fibroblast growth factor (FGF) and vascular endothelial growth factor (VEGF)<sup>33</sup>. In 3D studies of VSMCs on poly(glycolic) acid (PGA) scaffolds and type I collagen sponges, it has been reported that cyclic strain significantly increased the production rates of elastin and collagen and the application of

cyclic strain for 10 weeks induced a significant increase in cell alignment, as compared with control tissues<sup>34</sup>.

As would be anticipated, scaffolds in tissue engineering are a fundamental constituent in regulating cell behavior. Thus, the next section discusses types of scaffolds and their applications in tissue engineering. This information will guide the reader to specific scaffold modifications for the purpose of controlling VSMC behavior.

### **1.3 Scaffolds in Tissue Engineering**

Tissue engineering scaffolds provide a temporary or permanent support for cells and guide tissue maturation, and can be fabricated from naturally occurring materials or synthetic polymers. The choice of the type of scaffold used is dependent upon its tissue engineering application and, numerous design criteria exist. For example, scaffolds should have suitable surface chemistry to promote cellular attachment, migration, and proliferation<sup>35</sup>. Scaffolds should also exhibit appropriate pore size and high pore interconnectivity to promote cell infiltration and vascularization, and should have a controllable degradation rate synchronized with tissue growth and ECM production<sup>35</sup>. Furthermore, scaffold material and degradation products must not be cytotoxic, immunogenic, should not induce inflammatory or thrombogenic responses, and should meet regulatory standards<sup>2</sup>. Ease and cost of manufacturing, ability for mass production, and material stability are also significant engineering considerations. It is of importance to select a material that closely matches the properties of the tissue to be designed; soft tissues such as skin, tendon, blood vessels and heart valves are generally composed of

soft natural or synthetic polymers, while those for hard tissues such as bone and dentine are composed of ceramics, composites and rigid polymers<sup>36</sup>. Scaffolds are often designed in various shapes and sizes depending on their specific application.

### 1.3.1. Scaffolds from Natural Materials

Natural polymers are either modified polysaccharides such as cellulose, chitosan, and dextran, or ECM proteins such as collagen and fibrin<sup>37</sup>. Collagen and fibrin-based constructs have been used to engineer blood vessels, components of aortic valve cusps, and heart valve leaflets. Decellularized matrices have been used as natural scaffolds<sup>38,39</sup>, although there have been considerable challenges, including poor repopulation *in vivo*<sup>35</sup>. Incomplete removal of cellular debris after enzymatic digestion may compromise proper cell infiltration, and can result in immunological responses for allograft or xenograft scaffold sources. The risk of calcification has been an issue, and the mechanical properties of the native tissue are often compromised in the decellularization process<sup>40</sup>. Small intestine submucosa (SIS) is a resorbable natural acellular scaffold whose main component is collagen type I has shown to promote cell migration and spatial arrangement<sup>41</sup>. Mendelson and Schoen further elaborated that the success of SIS is attributed to the presence of cytokines and growth factors VEGF and TGF- $\beta$ <sup>40</sup>. The advantage of scaffolds fabricated from naturally occurring materials is that they could serve as a source of biological cues and cell signaling molecules that can promote cell attachment and proliferation – a hurdle for synthetic scaffolds without the addition of adhesion factors or other bioactive molecules. However, mechanical properties and degradation rates are difficult to control in natural scaffolds. Other drawbacks for natural

matrices, such as collagen, is the need to be cross-linked (fixed) in order to reduce the risk of an immunological response<sup>37</sup>.

### **1.3.2. Synthetic Scaffold Materials**

One major advantage of using synthetic matrices is the ability to design and chemically manipulate the material structure in order to achieve desirable mechanical properties and biodegradation rates<sup>37</sup>. Furthermore, physical and mechanical properties of synthetic scaffolds are more reproducible than natural scaffolds. However, slow or incomplete polymer degradation can give rise to tissue inflammation<sup>40</sup>. Degradation products such as lactic acid or butyric acid are generated with polyester hydrolysis, and cells exposed to this highly acidic region can be damaged or become necrotic especially during long culture times. Some common biodegradable synthetic polymers include poly(glycolic acid) (PGA), poly(lactic acid) (PLA) and their copolymers (PLGA), polyanhydrides, polyesters, polyurethanes, polyhydroxybutyrates (PHB), polydioxanone, and poly  $\epsilon$ -caprolactone. Biodegradable synthetic polymers such as PGA, PLA and their copolymers, poly(p-dioxanone), and copolymers of trimethylene carbonate and glycolide have been used in a number of clinical applications including resorbable sutures, drug delivery systems and orthopaedic fixation devices such as pins, rods and screws<sup>42</sup>. Polyurethanes have a low elastic modulus compared with other polyesters, making them desirable for soft tissue applications. PHBs are biocompatible, easily mouldable, and have high elasticity and mechanical strength, all of which are useful characteristics for soft tissue engineering<sup>43</sup>.

### **1.3.3. Biomimetic Scaffolds**

The complex signals experienced by cells include biochemical molecules (proteins, hormones, growth factors), mechanical forces, and cell-cell interactions. Biomimetic scaffolds offer a means to mediate and enhance cell-material interactions for tissue engineering, and can be fabricated by modifying (either chemically or physically) synthetic polymers with bioactive peptides, growth factors or biomolecules.

Alterations in the bulk chemistry of a polymer can consequently affect the mechanical properties of the polymer whereas surface modification of polymers with biomolecules will not extensively compromise the mechanical integrity of scaffolds<sup>44</sup>. Physically adsorbed bioactive molecules on a synthetic polymer have the disadvantage of being leached from the polymer into the surrounding media. In a perfusion system, one would observe the gradual loss of the bioactive compound. The covalent attachment of bioactive molecules on the synthetic polymer overcomes this problem; however, it may be difficult to chemically attach the desired molecule, especially without affecting its biological activity<sup>44</sup>.

#### **1.3.3.1. Fibronectin and RGD**

Cellular interaction with adhesion proteins in the ECM influences the morphology, motility, gene expression, and ultimately the survival of cells<sup>45</sup>. Since the discovery of the cell adhesion RGD sequence in fibronectin (FN) in 1984<sup>46</sup>, there has been considerable research to covalently attach this protein to synthetic polymers to impart biomimetic properties. As mentioned earlier, FN has also been shown to promote the synthetic phenotype in VSMCs in 2D culture.

Fibronectin is a 500 KDa glycoprotein, structurally a dimer of two anti-parallel subunits linked by a disulfide bridge at the C-terminus<sup>47</sup>. It is found in blood plasma and extracellular matrices, and each subunit is comprised of specific binding domains for integrins, collagen, heparin, and fibrin. It is through these domains that FN is able to mediate cell attachment and proliferation on various substrates<sup>47</sup>. The two distinct regions in fibronectin that possess cell binding activity are III<sub>9-10</sub> and III<sub>14-V</sub>; the adhesive motif sequence RGD is located in III<sub>10</sub>, while the LDV adhesive motif is found in the CS1 region of III<sub>14-V</sub><sup>47</sup>. Please refer to Table 1 for a list of integrins and their interaction site with FN.

**Table 1. Fibronectin-binding integrins and the key recognition site in fibronectin for binding. Table adapted from <sup>47</sup>.**

Integrin Receptor	Binding site in Fibronectin
alpha3β1	RGD
alpha5β1	RGD
alpha8β1	RGD
alphaVβ1	RGD
alphaVβ3	RGD
alphaIIbβ31	RGD
alphaVβ6	RGD
alpha4β1	LDV in CS1
alpha4β7	LDV in CS1

Instead of FN, many studies have immobilized the short chain RGD peptide to polymers through an amide bond between an activated surface carboxylic acid group on the polymer and a nucleophilic N-terminus of the peptide (reviewed in detail in <sup>48</sup>). The choice between using a protein versus a shorter peptide sequence in engineering

biomimetic scaffolds can be difficult, as both options have positive and negative aspects to them. For example, the whole proteins must be isolated and purified from other organisms, and may induce undesirable immune responses. Proteins are also subject to proteolytic degradation, thereby limiting their long-term use<sup>48</sup>. Proteins (either adsorbed or immobilized on a synthetic polymer) experience hydrophobic forces different from their native environment thus any resulting conformational change in the protein may alter the presentation of key motifs, if not bury them. This would reduce the effective biological activity of biomimetic scaffolds. Small peptides, on the other hand, tend to have higher stability towards heat sterilization, pH variation, storage, and are easier to characterize and are cost effective<sup>48</sup>. Furthermore, since peptides occupy less space than proteins, peptides can be packed at higher densities on the modified scaffold surface<sup>48</sup>. Still, a single protein contains several motifs that are recognized by cells whereas a small peptide fragment represents only a single motif. For the case of fibronectin, it has been shown that the protein contains a multitude of recognized domains other than the RGD motif, all of which play a role in the complexity involved in signaling pathways. For example, the REDV sequence in the CS5 region (a total of 20 amino acids) of fibronectin supports endothelial cell attachment and spreading<sup>49</sup>. REDV motifs incorporated into polypeptides did not have the ability to mediate attachment and spreading of endothelial cells but, upon inserting of all 20 amino acids of the CS5 region into the polypeptide, including the REDV sequence, it restored endothelial cell adherence<sup>50</sup>. Cell migration requires that focal adhesions formed between the integrins and cell-binding ligands to cyclically break and re-form; otherwise cells are immobilized on the surface. Hence, when adhesion forces are dominating such as in high immobilization densities of RGD,

migration slows down<sup>49</sup>. Further investigation, however, has shown that cell migration and spreading is higher on fibronectin immobilized surfaces compared to solely the RGD motif suggesting that fibronectin plays an additional role through other synergistic binding domains such as PHSRN<sup>49, 51, 52</sup>. Thus the complexity in the fibronectin molecule and its domains involved in cell signaling suggest that immobilizing the protein instead of a single motif may be more advantageous. From a blood vessel tissue engineering standpoint, it is also the entire fibronectin protein that holds significant importance. Fibronectin promotes the synthetic phenotype in VSMCs which is essential to deposit elastin and other key ECM components in developing tissue engineered constructs, and as described earlier, the contractile phenotype would not suffice.

#### **1.4 Techniques in Scaffold Fabrication**

Several conventional techniques in scaffold design and fabrication exist. These include gas foaming<sup>53</sup>, fiber bonding<sup>54</sup>, freeze drying<sup>55</sup>, and solvent casting-particulate leaching<sup>56</sup>. The gas foaming technique eliminates the need for organic solvents in making scaffolds. In the reported procedure, solid discs of PGA, poly(lactic acid) (PLA), or poly(lactic-co-glycolic acid) (PLGA) are first placed in a high pressure CO<sub>2</sub> chamber (5.5 MPa) for three days. The chamber pressure is then rapidly decreased to atmospheric pressure, resulting in the nucleation and expansion of dissolved CO<sub>2</sub> out of the polymer discs resulting scaffold porosities can be up to 93% with pores sizes of up to 100 μm<sup>53</sup>. Nonetheless, the high temperatures involved in the procedure inhibit the incorporation of biomolecules, and the pore structures do not have high interconnectivity<sup>57</sup>.

In the fiber bonding technique, polyglycolic acid (PGA) fibers are immersed in a Poly-L-Lactide Acid (PLLA) solution, and the solvent is evaporated allowing the PGA fibers to embed in the PLLA. This composite is heated above the melting temperature of both polymers. The PLLA melts first, filling the voids left by the fibers, and as the PGA begins to melt, the fibers at the cross-points melt together and weld. The PLLA is then dissolved out from the composite in methylene chloride, leaving behind porous foam. This fabrication technique creates scaffolds with porosities up to 81% and pore diameters of up to 500  $\mu\text{m}$ <sup>53</sup>. However, these scaffolds are not even capable of withstanding contractile forces exerted by cultured smooth muscle cells, and strict polymer requirements (immiscibility and similar melting points) makes it difficult to apply to other polymers<sup>58</sup>.

With the freeze drying method, the polymer is dissolved or emulsified in water to the desired concentration and the solution is then lyophilized under high vacuum to remove the solvent<sup>58</sup>. The resulting foams have capillary or leaflet pore structures which are not suitable for cell-seeding. A slight modification of this technique was first proposed by Whang et al.<sup>55</sup>. The group dissolved PLGA in methylene chloride, added distilled water to form an emulsion, and cast the emulsion into a mold. The construct was quenched in liquid nitrogen and freeze dried at  $-55^{\circ}\text{C}$  in order to remove the water and solvent. The resulting scaffolds had high porosities of up to 95% but very small pore sizes (13-35  $\mu\text{m}$ ). Furthermore, the use of organic solvents in this procedure prohibits the use of bioactive molecules.

The solvent casting and particulate leaching (SCPL) technique for scaffold fabrication allows for controlled porosity and pore size, and can be applied to many polymer types<sup>58</sup>. In the procedure (please refer to Figure 1), the polymer is first dissolved in a solvent. The polymer solution is then cast into a mold containing a porogen, where the porogen is conventionally a water soluble salt. The solvent is then evaporated, and the porogen is leached out in water. The resulting scaffold's porosity and pore interconnectivity can thus be controlled by the porogen size and ratio of polymer to porogen. In order for this technique to work, the solvent dissolving the polymer must not dissolve the porogen, and the solvent dissolving the porogen must not dissolve the polymer. The earliest reports of this technique used PLA dissolved in chloroform and sodium chloride as the porogen<sup>56</sup>. Since then, a wide range of porogen types including sugar, gelatin, and paraffin have been explored<sup>59</sup>.

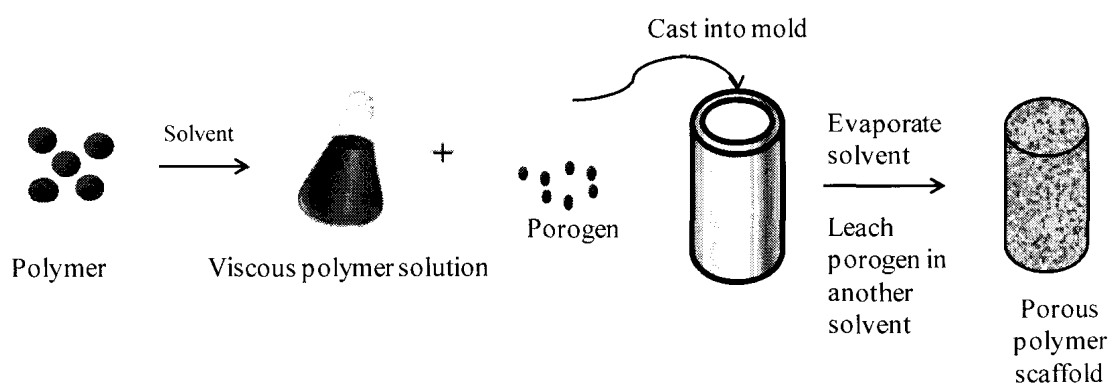


**Figure 1. Schematic of the solvent-casting particulate leaching scaffold fabrication method.**

Two recently emerging techniques in scaffold fabrication are solid freeform (rapid prototyping) and electrospinning. Solid free-form (SFF), also referred to as rapid prototyping, generates a physical 3D scaffold by repeated layer-by-layer deposition of 2D cross-sectional data obtained from a computer-aided design (CAD) models<sup>60</sup>. This

method allows for detailed control over the scaffold architecture. Types of SFF systems include stereolithography, selective laser sintering, laminated object manufacturing, three-dimensional printing and fused deposition modeling<sup>61</sup>. The details of each of these techniques are outside the scope of this thesis. Although tissue engineers have had increasing interest in the SFF method for scaffold fabrication, the main challenge that needs to be addressed is the limited range of materials that can be used. Each of the SFF procedures listed above require a specific form of the polymer (such as filament, powder, solution, or pellet), the choice of material must be compatible with the technique used.

The native environment exposed to cells is 1 to 2 orders of magnitude smaller than the cell itself, and in order to mimic this, more research is being conducted in developing scaffolds that have nanofiber dimensions<sup>62</sup>. Electrospinning is a technique that can be used to fabricate such scaffolds<sup>63</sup>. Generally, an electric potential is applied between a polymer solution source (usually in a syringe) and the collector plate. A charge begins to accumulate onto the surface of a polymeric solution droplet at the end of the syringe, and once the force of the electric field overcomes the cohesive force of the solution, an electrically charged jet of polymer solution is ejected towards the collector plate and elongated in the process. The solvent evaporates as the jet solidifies and deposits as fine fibers on the collector plate. Electrospun scaffolds typically are difficult to reproduce as the fibers are created randomly as well as the resulting pores<sup>62</sup>. Furthermore, pore sizes are too small for cells to infiltrate<sup>63</sup>.

The aforementioned scaffold processing methods have their advantages and disadvantages. For the purpose of this research, the SCPL method is favored as it allows for versatility in choice of polymer type, pore size and porosity. Scaffold fabrication is also cost-effective and reproducible.

### **1.5 Immobilization Strategies of FN onto 3D Scaffolds**

Different approaches to conjugate FN on various types of synthetic polymers have been reported, although the majority of these studies were conducted on films rather than on porous 3D scaffolds that would ultimately be used to fabricate viable tissues. Poly(ethylene terephthalate) (PET) membranes have been covalently grafted with FN, and results have demonstrated accelerated hepatocyte adhesion on FN grafted PET membranes in comparison to PET alone and FN adsorbed on PET<sup>64</sup>. In the reported procedure, PET membranes were oxidized in a solution of  $\text{KMnO}_4$  in  $\text{H}_2\text{SO}_4$  to generate COOH functionalities on the membrane, which were subsequently activated in an N-ethyl(dimethylaminopropyl) carbodiimide (EDC) solution and incubated in an FN solution in PBS. In another described technique to conjugate FN to PET, PET film surfaces were first aminated in ethylenediamine solution, reacted with glutaraldehyde, and finally reacted with FN<sup>65</sup>. Interestingly, the study demonstrated that the adsorbed FN on PET exposed more RGD domains and better supported cell adhesion in comparison to high concentrations of FN conjugated on PET. Atomic force microscopy (AFM) studies suggested that intermolecular interactions between FN caused fibrillogenesis, a morphological fibril arrangement of FN that is not conducive to cell attachment.

FN has been immobilized on poly(lactic acid) (PLA) films<sup>66</sup>. The PLA surfaces were first hydrolyzed with NaOH in order to generate COOH groups, which were then activated in EDC and exposed to FN solution to form FN-functionalized PLA. These films were shown to greatly enhance the initial attachment of human gingival fibroblasts. Silicone derived artificial cornea and retinal patches have been functionalized with FN and cell studies revealed that adsorption of FN on silicone surfaces only poorly improved cell growth, whereas cells grew to confluence on the chemically immobilized FN layer<sup>67</sup>. In the reported procedure, silicone surfaces were plasma gas treated in the presence of acrylic acid (AA) in order to graft poly acrylic acid. FN conjugation was achieved by reacting the COOH groups of the PAA with EDC and an FN solution.

In an approach to reconstruct 3D tissue, cellulose hollow fiber bundles were functionalized with FN by first activating hydroxyl groups on the cellulose with tresyl chloride and then immersing the fibres in FN solution<sup>68</sup>. Bovine coronary artery smooth muscle cells (BCASMCs) were shown to proliferate and form multicellular layers on the hollow fibres. This activation method was also used to functionalize titanium materials for dental implants<sup>69</sup>. In the proposed technique, terminal OH groups of titanium discs were activated with tresyl chloride, and immersed in FN solution for the direct attachment of FN. Unfortunately, cell studies using gingival fibroblasts revealed that FN conjugated titanium did not influence initial cell attachment, although collagen conjugated titanium surfaces did<sup>70</sup>. A notable procedure for immobilizing FN on a PEO-containing tri-block copolymer (Pluronic™) has been reported<sup>71</sup>. The terminal hydroxyl groups of the PEO segment were modified with a pyridyl disulfide (PDS) group and FN was thiolated using a similar procedure. A subsequent reaction between the thiolated FN

and the PDS group on the PEO generated the FN functionalized polymer. Cell studies demonstrated that the FN conjugated Pluronic™ supported fibroblast attachment, spreading and proliferation, where the original polymer failed to do so even in the presence of serum containing media. FN has been grafted on electrospun poly(L-lactide-co-caprolactone) (PLLC) nanofibrous scaffolds<sup>72</sup>. The reported technique involved the aminolysis of the scaffold in a 1,6-hexanediamine/propanol solution and subsequent reaction with GA. The glutaraldehyde crosslinker was then reacted with FN. The FN conjugated scaffolds enhanced collagen synthesis and esophageal endothelial cells viability in compared to PLLC alone.

Certain protein conformations may bury the cell adhesion motif, and thus the bioactivity of FN is dependent upon the route of conjugation. In order to investigate this, PTFE films have been FN conjugated using several cross-linker types<sup>73</sup>. First PTFE films were treated by a radiofrequency glow discharge (RFGD) ammonia plasma to introduce amino groups on the surface. These groups were then reacted with different spacer molecules such as glutaric anhydride (GA) or sulfo-succinimidyl-4-(*p*-maleimidophenyl) butyrate (sulfo-SMPB) and subsequently conjugated with FN. Subsequent studies demonstrated the importance of spacer type on the bioactivity of FN immobilized PTFE films. Cell adhesion and RGD motif availability was shown to be greater using a GA cross-linker compared to sulfo-SMPB. The chemical conjugation schemes for these two cross-linkers targeted different sites on FN: GA reacts with the primary amines on FN while sulfo-SMPB reacts with sulfhydryl groups in cysteine containing amino acids in FN. There are only 3 free cysteine residues per subunit of FN in comparison to 76 lysine (free amine containing amino acid) residues per subunit of FN, and thus there are far more possible

conjugation sites for cross-linkers targeting free amines<sup>74</sup>. In a similar study, another group investigated the effect of selective spacer arms on the conformation of fibronectin conjugated to plasma treated fused silica (PTFS)<sup>74</sup>. In this study, FN was coupled to PTFS using either GA or SMPB. AFM analysis showed different topographies and surface roughness for FN immobilized on each type of spacer arm for same grafting densities. Results showed that bovine aortic endothelial cells had higher adhesion with the GA spacer arm compared to the SMPB spacer arm. FN height and diameter distribution were found to be significantly larger with the GA linker. These results are an indication that the immobilization strategy has a significant effect on protein conformation and activity, and that using a GA spacer arm is preferable spacer arm over SMPB. To further elaborate the effects of FN conjugation strategy on bioactivity, FN was directly attached to the polymer surface without any spacers. Generally, a spacer arm tethering a protein can allow for a greater degree protein mobility in order to allow it to present itself in an active form<sup>75</sup>. Perhaps the protein in the latter is freer and, more amenable to its active conformation than when it is in such close proximity to the polymer surface.

In the aforementioned studies, FN conjugation strategies have been performed on 2D substrates. There are only a few studies reporting FN conjugation on 3D scaffolds. One of such studies was conducted by Lu et al.<sup>76</sup>. 3D porous scaffolds with complex internal architectures and spatial patterning were fabricated using the rapid prototyping technique of microstereolithography. A UV light source, digital mirror device masking agent, and a photo-crosslinkable polymer, a poly(ethylene glycol) diacrylate and methacrylic acid solution were used to generate the scaffolds. The COOH groups were activated in an

EDC/sulfo-NHS and FN was added to the mixture to form the final FN conjugated 3D scaffold. The targeted cell type in this study was marrow derived stem cells and the results demonstrated that stromal cells can be successfully attached to the functionalized scaffolds and in the presence of osteogenic medium, transformed into osteoblasts. Cells did not even attach to the control scaffolds, which is not surprising due to the hydrogel nature of the scaffold.

In another report, FN was conjugated on a fibrous 3D mesh of nonwoven PET via a gluaraldehyde cross-linker<sup>77</sup>. The target cells used in the study were hematopoietic stem cells, and results showed a 100-fold increase in cell expansion in comparison to the 2D FN-immobilized PET films. Thus the mimicry of the 3D structure of ECM is also clearly important in regulating cell behavior, and studies on 2D films are not always adequate to gain information about cell-material interactions. A recently reported technique describes the fabrication of 3D cylindrical scaffolds from PCL-PEG-PCL block copolymers and subsequent FN conjugation{Bramfeldt, 2008 #348}. In the procedure, the polymer was first chemically aminolyzed, incubated in dimethylpimelimidate (a cross linking reagent) and reacted with a FN solution. Studies smooth muscle cell seeding increasing pore size improved cell numbers on the FN conjugated scaffolds.

Thus, to date, there are very few attempts to conjugate FN onto 3D porous scaffolds and systematic studies on FN conjugation to 3D tissue engineering scaffolds is lacking.

## 1.6 Objectives and Rationale

Scaffolds play an essential role in scaffold-guided tissue engineered constructs as they interface directly with cells. One of the most widely used synthetic scaffolds for tissue engineering are polyurethanes, an elastomeric material suitable for soft tissue applications, such as vascular tissue engineering<sup>79</sup>. In spite of their excellent mechanical properties, polyurethanes exhibit little bioactivity. To make their surfaces more conducive to cell attachment and spreading, immobilization of proteins such as cell adhesive proteins or peptides is a promising approach<sup>80</sup>. As aforementioned, fibronectin is a multiple domain protein containing the cell adhesion sequence RGD, as well as the ability to promote the synthetic phenotype in vascular smooth muscle cells. Thus, to create biomimetic scaffolds for vascular tissue engineering purposes, FN is an attractive candidate for conjugation to polyurethanes.

The principle objectives of this study were to:

- Fabricate highly porous 3D polyurethane scaffolds;
- Establish a protocol to graft acrylic acid spacers on the 3D scaffolds and conjugate the protein fibronectin;
- Conduct comprehensive characterizations of FN conjugated scaffolds and intermediates;
- Assess the interaction of these biomimetic 3D scaffolds with vascular smooth muscle cells.

The long term goal is to allow these cell-seeded, biomimetic scaffolds to mature in a perfusion bioreactor system where the construct will be provided with a constant supply of nutrients and pulsatile stimulation.

## CHAPTER 2

### 2 Materials and Methods

#### 2.1 Materials

Medical grade poly(carbonate urethane) (PCU), kindly supplied by the Polymer Technology Group (Berkeley, CA), was used as the scaffold material in this work. Please refer to Figure 2 for the chemical structure of the PCU. Dimethylformamide (DMF), ammonium chloride ( $\text{NH}_4\text{Cl}$ ), cerium ammonium nitrate ( $\text{Ce}(\text{NH}_4)_2(\text{NO}_3)_6$ ), copper nitrate ( $\text{Cu}(\text{NO}_3)_2$ ), acrylic acid, toluidine blue, N-hydroxysuccinimide (NHS), 4-morpholineethanesulfonic acid (MES), and phosphate buffered saline (PBS) were purchased from Sigma Aldrich (Milwaukee, WI). Acetic acid was obtained from Caledon Chemicals (Georgetown, ON, Canada) and ethyl(dimethylaminopropyl) carbodiimide (EDC) from Fluka (Milwaukee, WI). Paraformaldehyde was purchased from EMD Chemicals (Gibbstown, NJ). The BCA Assay Kit was purchased from Pierce Thermo Scientific (Rockford, IL). Human plasma fibronectin, rabbit polyclonal IgG primary antibody and Texas Red conjugated-goat anti-rabbit IgG secondary antibody were purchased from Santa Cruz Biotechnology (Santa Cruz, CA). Smooth muscle basal medium (Clonetics SmBM) and human coronary artery vascular smooth muscle cells were purchased from Lonza Walkersville Inc. (Walkersville, MD). Alexa<sup>TM</sup> Fluor 568-conjugated phalloidin and Hoechst 33342 were purchased from Invitrogen (Burlington, ON).

## 2.2 Scaffold Fabrication

Scaffolds were fabricated using a pressure differential solvent casting-particulate leaching method (SCPL). The  $\text{NH}_4\text{Cl}$  particles were crushed and sieved to 180-210  $\mu\text{m}$  using standard testing laboratory sieves (VWR International, Mississauga, ON) and packed into a cylindrical mold (5.5 mm diameter, 8 cm height). A 15% (v/v) viscous solution of PCU in DMF was poured over the particle bed and forced through the apparatus (please refer to Figure 3) using an air supply line. The mold was removed from the apparatus and the cylindrical construct was pushed out of the mold to allow the solvent to evaporate in a fume hood for 2 days. The  $\text{NH}_4\text{Cl}$  particles were then leached out of the construct by immersing the scaffold in a beaker of distilled water for 2 days. The cylindrical porous 3D scaffolds fabricated were then sliced into 1 mm discs with a sharp rotating blade for further studies.

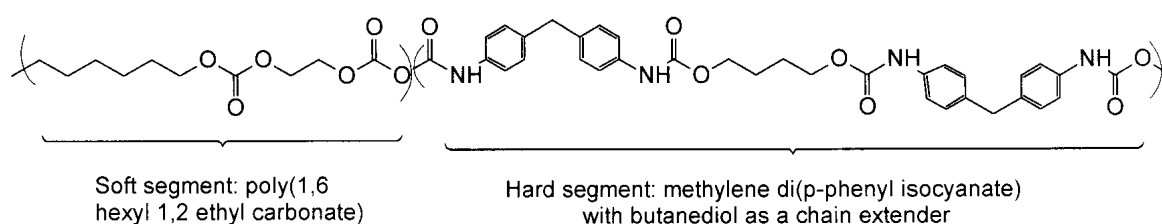


**Figure 2. Chemical structure of Bionate 80A, the polycarbonate urethane used in this work.**

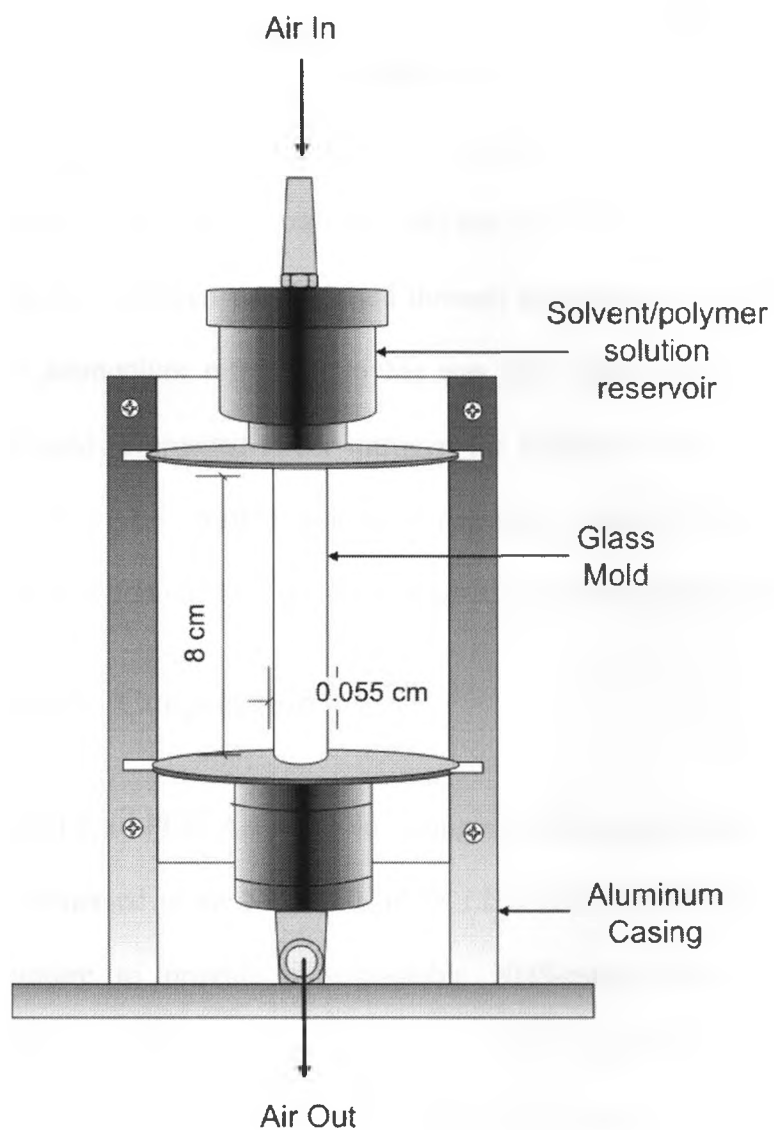


**Figure 3. Schematic drawing of the pressure differential scaffold casting apparatus.** The solvent/polymer solution is forced through the tubular glass mold that is packed with porogen. The glass mold is then removed from the apparatus in order to process the scaffolds.

### **2.3 Acrylic Acid Grafting onto Porous 3D Polyurethane Scaffolds**

Grafting of acrylic acid (AA) onto 3D scaffolds was carried out using a ceric ion initiator as described in polymer syntheses literature<sup>81</sup>. Scaffolds (1 mm thick discs) were first immersed in a solution of copper nitrate (0.1 M) and AA (ranging from 1 M to 18 M) at ambient temperature. Nitrogen was bubbled through the mixture for 20 min to remove oxygen. Cerium ammonium nitrate (0.06 M) was then added to the mixture and the reaction was allowed to proceed under nitrogen for different times (30 min to 8 h) at ambient temperature. AA grafted scaffolds (hereafter called PCU-AA) were then removed from the reaction solution and were washed copiously with distilled water.

### **2.4 Fibronectin Conjugation**

FN was conjugated onto PCU-AA scaffolds using a two-step procedure: First, PCU-AA scaffolds were immersed in an NHS (50 mM), EDC (25 mM) solution for 15 min at ambient temperature to provide a semi-stable NHS-ester (PCU-AA-NHS). These scaffolds were subsequently immersed in an MES buffer (40 mM, pH 4.1) containing 0.1 to 0.5 g/mL FN and stirred using a magnetic stirrer for 24 h at ambient temperature to give fibronectin conjugated 3D scaffolds (PCU-AA-FN). Grafting and conjugation reactions are shown in Figure 4. As a control, PCU and PCU-AA scaffolds were immersed in the same FN concentration for the same time as the conjugation reactions.

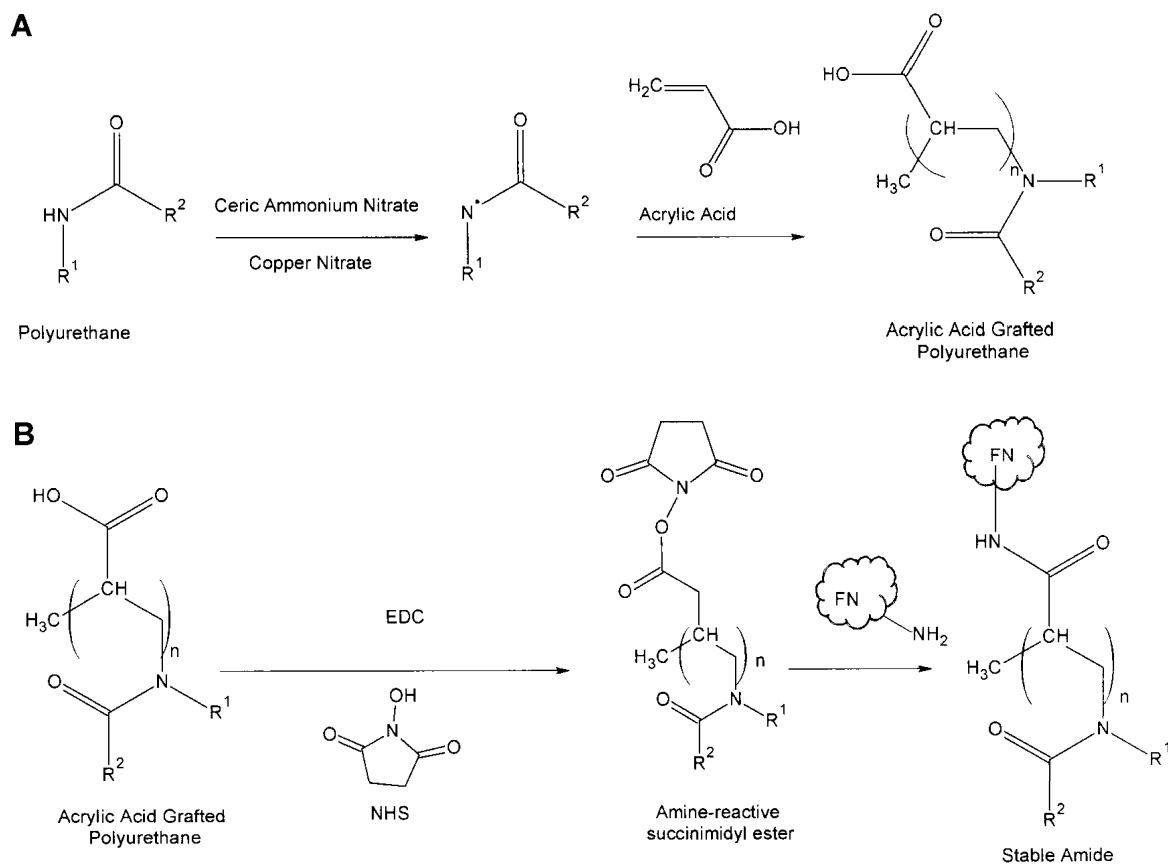


**Figure 4. FN conjugation scheme onto 3D porous PCU scaffolds.**

(A) The first step involves grafting AA on the urethane moiety. (B) The peptide coupling in the second step is accomplished using EDC as an activator and NHS as an intermediate stabilizer.

## **2.5 Scaffold Characterization**

### **2.5.1. Scanning Electron Microscopy (SEM)**

Scaffold morphology and pore structures following fabrication and after each of the reaction steps (grafting, activation and conjugation) were visualized using SEM, (S-2600N, Hitachi, Japan). Samples were mounted on carbon-taped aluminum stubs and gold-sputtered at 15 mA for 1.5 min prior to analysis.

### **2.5.2. Fourier Transform-Infrared Microscopy (FT-IR)**

FT-IR was used to monitor reaction progress on 3D scaffolds. FT-IR spectra were obtained using a Bruker Vector 22 spectrophotometer (Milton, ON). For each sample, 64 scans at  $4\text{ cm}^{-1}$  resolution were captured.

### **2.5.3. Toluidine Blue (TB) Assay**

The carboxylic acid groups on the PCU-AA scaffolds were quantified using TB assay. TB (Fig. 5) is known to form a complex with acid groups in a 1:1 ratio at a basic pH and can be dissociated under acidic conditions<sup>82</sup>. The number of carboxylic acid groups grafted onto the PCU were calculated under the assumption that every  $\text{COO}^-$  binds to a single TB molecule. PCU-AA scaffolds were immersed in a  $5 \times 10^{-4}$  M solution of TB at pH 10 for 20 min. Following this, the scaffolds were rinsed three times with distilled water to remove unbound TB and were air-dried. PCU-AA scaffolds were then exposed to 3 mL of 50% (v/v) acetic acid solution for 2 h and the optical density of the extracted TB dye was measured at 633 nm using a Beckman Coulter DU 520 UV-Vis Spectrophotometer (Mississauga, ON). A calibration curve correlating toluidine blue

concentration and absorbance was prepared in order to determine the concentration of dye extracted from the scaffolds.

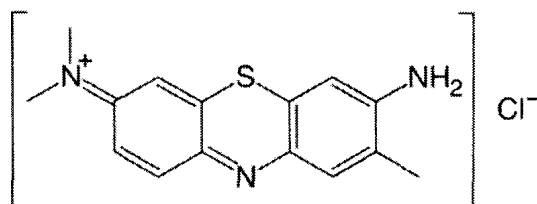


**Figure 5. Chemical structure of toluidine blue.**

Under basic conditions, the carboxylic acid groups on the scaffold are deprotonated ( $\text{COO}^-$ ), and thus interact with the positively charged dye.

#### **2.5.4. X-Ray Photoelectron Spectroscopy (XPS)**

High resolution XPS scans for oxygen, nitrogen, and carbon were obtained to confirm changes in key functional groups, while survey scans were used to provide information about the elemental composition after each reaction step. XPS data were obtained using a Kratos Axis Ultra spectrometer (Manchester, UK) using an analysis spot size of  $400 \times 700 \mu\text{m}^2$  and monochromatic Al  $K\alpha$  as the x-ray source. The base pressure in the analytical chamber was maintained at  $6.6 \times 10^{-11}$  kPa, and measurements were made at a  $90^\circ$  take-off angle. Spectra were obtained and analyzed using CasaXPS software (version 1.0.0.1).

#### **2.5.5. Immunofluorescence Microscopy**

Immunofluorescence studies were performed in order to visualize FN on PCU-AA-FN scaffolds. Scaffolds were sliced into 0.8 mm thin discs with a sharp rotating blade and were incubated with the primary antibody against fibronectin (1:100 dilution) in PBS for 60 min at room temperature. Scaffolds were then washed with three changes of PBS for 5 min each, and incubated in Texas-red conjugated secondary antibody (1:200 dilution) in

PBS for 45 min. Scaffolds were mounted on glass slides with a coverslip and Trevigen mounting medium, and examined with a Leica DM-IRB fluorescence microscope. PCU scaffolds were shown not to auto-fluoresce in the red wavelength, and as a background control, PCU-AA scaffolds were exposed to the same staining procedure.

### **2.5.6. Bicinchoninic Acid (BCA) Assay**

PCU-AA-FN conjugated (0.5 mg FN) and PCU-AA FN adsorbed (0.5 mg FN) scaffolds were prepared and rinsed three times for 5 min in PBS in order to remove loosely adsorbed FN and MES buffer. FN was then leached from PCU-AA-FN conjugated (0.5 mg FN) and PCU-AA FN adsorbed (0.5 mg FN) scaffolds in PBS for time intervals between 6-48 h. Each scaffold was placed in fresh 2 mL PBS for each time interval. After 48 h any remaining adsorbed FN was extracted using 2% SDS and mild agitation for 1 h. FN leached from scaffolds was then quantified using the BCA Assay. This method involves the reduction of  $\text{Cu}^{2+}$  to  $\text{Cu}^{+}$  by proteins in an alkaline medium<sup>83</sup>. The resulting  $\text{Cu}^{+}$  ion chelates with bicinchoninic acid to produce a purple complex that absorbs strongly at 562 nm and is linear over broad protein concentrations (20-2000  $\mu\text{g/mL}$ ). The Working Reagent was made by combining 50 parts of BCA Reagent A with 1 part BCA Reagent B. Afterwards, 0.1 mL of the leached FN in PBS was mixed with 2 mL of the Working Reagent and incubated at room temperature for 2 h. Absorbances of the solutions were read at 562 nm using a Beckman Coulter DU 520 UV-Vis Spectrophotometer (Mississauga, ON). A calibration curve correlating FN concentration and absorbance was prepared in order to determine the unknown leached FN quantities from scaffolds.

## 2.6 Cell Work

Scaffolds were sliced to 0.8 mm thickness and mounted on glass coverslips with grease, and sterilized in 70% ethanol for 30 min. Dried scaffolds were seeded with human coronary artery vascular smooth muscle cells (passages 4-6) and maintained in SmGM in a humidified incubator containing 5% CO<sub>2</sub> at 37°C for 4 days. The cell seeding densities were counted with a hemocytometer. Cells on the scaffolds were then fixed at ambient temperature in 2% PFA in PBS for 10 min, and permeabilized in 0.5% Triton X-100 in PBS for another 10 min. After washing three times with PBS at 5 min each, cell-seeded scaffolds were incubated for 1 h at ambient temperature in Alexa Fluor-568 conjugated phalloidin in PBS (1:50), washed with PBS, and incubated for 10 min in Hoechst 33342 (20 µg/mL in PBS). Scaffolds were mounted on glass slides in Trevigen mounting media, sealed and analyzed with a Leica DM-IRB fluorescence microscope and a Zeiss LSM 410 confocal microscope.

# CHAPTER 3

## 3 Results

### 3.1 Chemistry and FT-IR Analysis

The FT-IR spectra of the PCU, PCU-AA, PCU-AA-NHS, and PCU-AA-FN scaffolds are shown in Figure 6. For the PCU scaffolds, the urethane N-H stretch appears as a strong narrow peak at  $3340\text{ cm}^{-1}$  (Figure 6A). Referring to Figure 4A, the first step in the reaction scheme involves the abstraction of the urethane hydrogen, followed by the radical polymerization of AA onto the urethane nitrogen using ceric ammonium nitrate as an initiator. Upon AA grafting (PCU-AA), the N-H peak is replaced by a broad O-H stretch in the region of  $3500\text{-}3000\text{ cm}^{-1}$  due to the grafted COOH groups, indicating that the urethane hydrogen is replaced by an acrylic acid residue (Figure 6B). The H-bonded C=O appears at  $1699\text{ cm}^{-1}$  and the free C=O appears at  $1740\text{ cm}^{-1}$ . On relative terms, the peak intensity of the H-bonded carbonyl decreases in the PCU-AA samples, which may be due to the absence of a proton donor for H-bonding interaction with the grafted AA groups. This observation is not unexpected, since the urethane hydrogen is abstracted during the grafting process. In the subsequent step of the reaction scheme, referring to Figure 4B, the grafted carboxylic acid functionalities were activated in EDC and reacted with NHS to yield a semi-stable, amine-reactive succinimidyl ester (PCU-AA-NHS). The PCU-AA-NHS spectrum (Figure 7C, arrow) shows a distinctive peak at  $1650\text{ cm}^{-1}$  which is assigned to the C=O stretch in the succinimidyl ester<sup>84</sup>. EDC alone is not

efficient as a protein coupling agent, as failure to react quickly with the amine terminus of the protein will result in hydrolysis and regeneration of the carboxyl group<sup>14</sup>. This is especially the case where the target protein concentration is low, as is the case in the present study, and EDC/NHS coupled reactions have been shown to significantly increase the conjugation yield than using EDC alone<sup>85</sup>.

In terms of conjugation strategy, the PCU-AA-NHS ester targets free amine groups, and it is possible that  $\alpha$ -amine groups on the N-termini of proteins are not entirely accessible to react. While only a few amino acids have free amine groups in their side chains (ex. lysine, arginine, glutamine), the  $\epsilon$ -amine of lysine has been shown to react significantly with NHS esters<sup>86</sup>. An FN molecule contains about 76 lysine residues per subunit<sup>74</sup> and thus there should be more than several target sites for the PCU-AA-NHS esters to react with FN. The amine-reactive NHS ester was then exposed to an acidic solution of FN in MES buffer, where it reacted with primary amines on the protein to produce FN conjugated 3D scaffolds (PCU-AA-FN). It is worthwhile to note that the succinimidyl ester peak was no longer observed indicating that the conjugation reaction was complete.

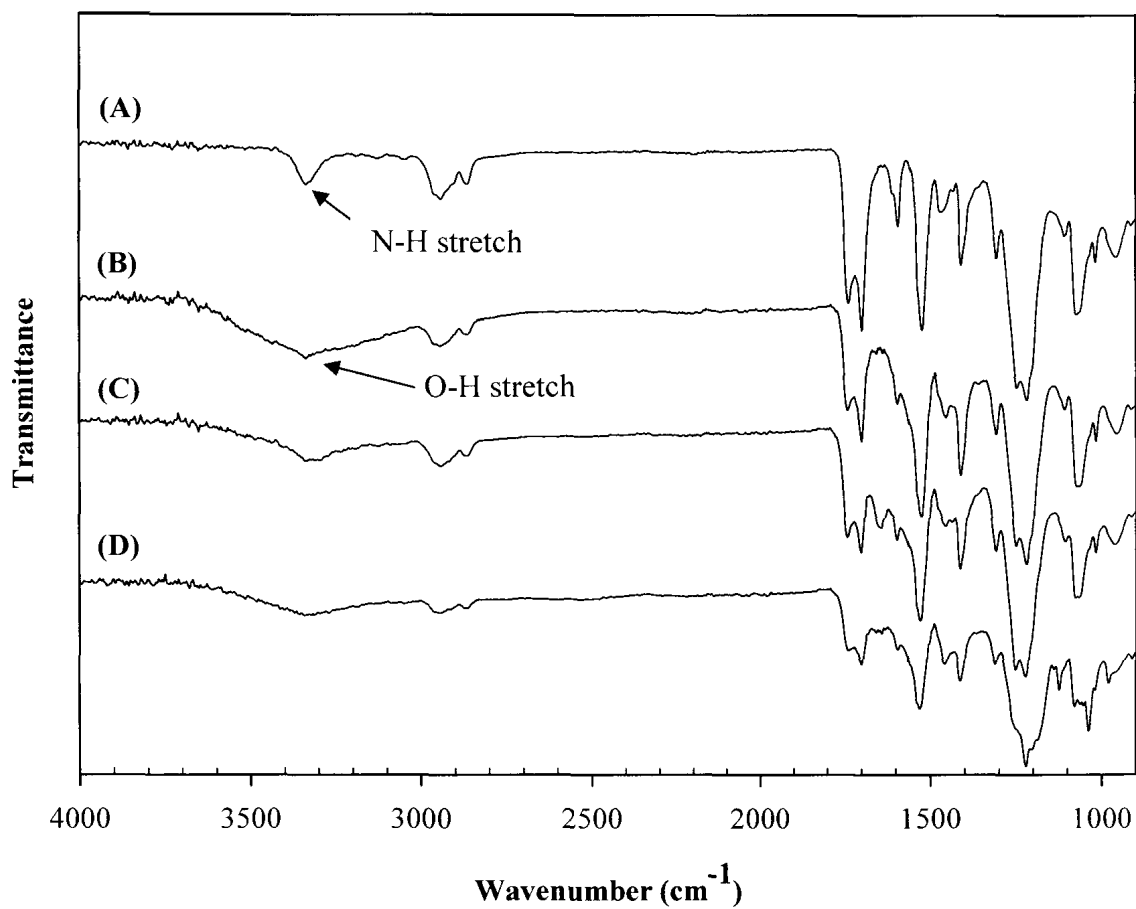


**Figure 6. FT-IR spectra of: (A) PCU; (B) PCU-AA; (C) PCU-AA-NHS; (D) PCU-AA-FN scaffolds.**

There are marked differences in the spectra below 1800  $\text{cm}^{-1}$ . For an expanded view of the 1800-1100 $\text{cm}^{-1}$  region of all scaffolds please refer to Figure 7.

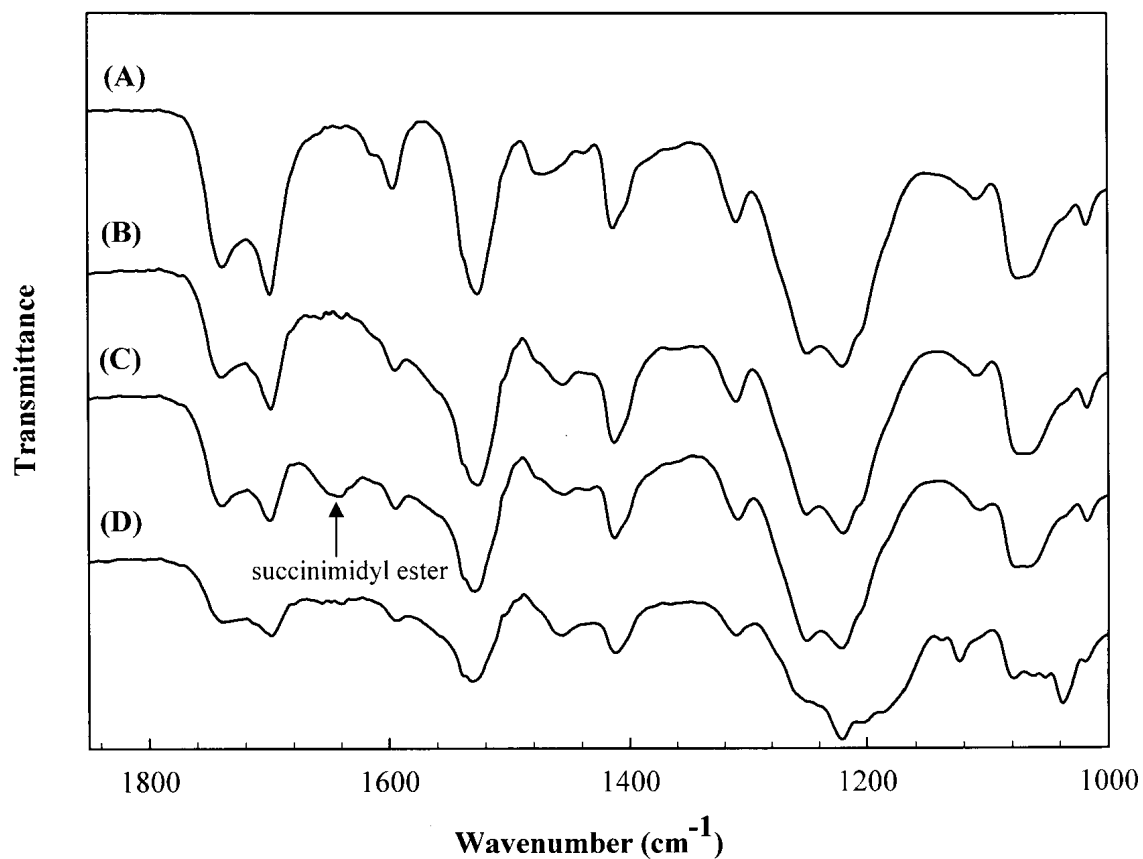


**Figure 7. Expanded view of the 1800-1000 cm<sup>-1</sup> region for (A) PCU; (B) PCU-AA; (C) PCU-AA-NHS; and (D) PCU-AA-FN scaffolds.**

The succinimidyl ester peak is visible only in (C) at 1650 cm<sup>-1</sup>. A separate close-up of PCU-AA-FN scaffolds is presented in Figure 8 in order to see distinct amide bands.

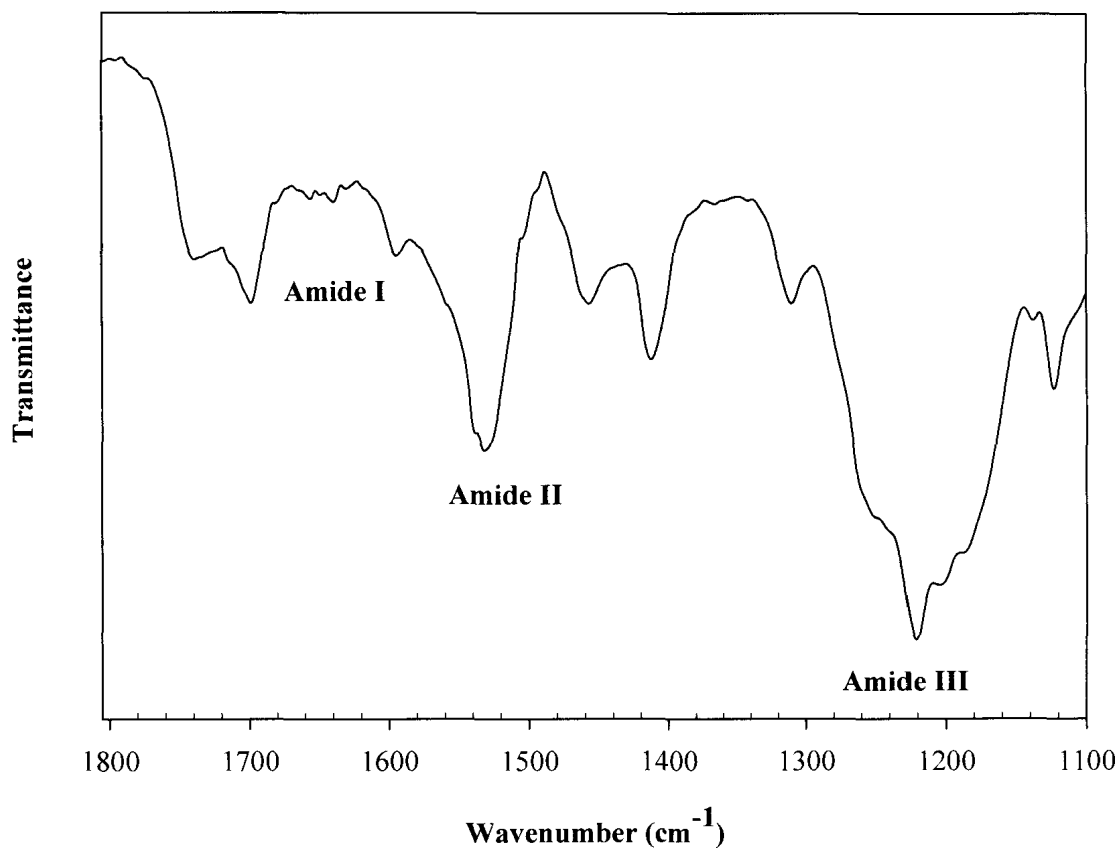


**Figure 8. Expanded view of FT-IR spectra for PCU-AA-FN scaffolds in the characteristic amide I, II, and III regions.**

The amide I bands are observed at 1638 and 1660, and 1680 cm<sup>-1</sup>, amide II bands are observed at 1540, 1530, and 1510 cm<sup>-1</sup> and amide III bands at 1310, 1265, and 1225 cm<sup>-1</sup>.

Detailed FT-IR studies have been conducted by Cooper et al.<sup>87</sup> on FN adsorbed onto polyurethane surfaces. They attributed changes in the absorbance in the 1740 -1720 cm<sup>-1</sup> region to the carbonyl stretching vibration of the COOH groups arising from the C-terminus of the protein as well as carboxylic acid-containing amino acid residues (Asp and Glu). As seen in Figure 7D there are visible differences in this region, and the peak at 1740 cm<sup>-1</sup> is noticeably broader.

Peaks in the regions of amide I (1700-1600  $\text{cm}^{-1}$ ), amide II (1580 - 1510  $\text{cm}^{-1}$ ) and amide III bands (1300-1200  $\text{cm}^{-1}$ ) were observed in these FN conjugated scaffolds that were markedly different than the aforementioned spectra (Figure 8). The peaks observed at 1638  $\text{cm}^{-1}$  and 1660  $\text{cm}^{-1}$  and a smaller band at 1680  $\text{cm}^{-1}$  are characteristic of amide I absorbances and have been previously reported<sup>87,88</sup>. The bands at 1638  $\text{cm}^{-1}$  and 1680  $\text{cm}^{-1}$  are generally assigned to the  $\beta$ -sheet structure, while the other observed peaks are considered to be unordered conformations<sup>87,88</sup>. There were three expected amide II bands observed at 1540, 1530, and 1510  $\text{cm}^{-1}$ , although their shifts were slightly different than what was previously reported (1550, 1532, and 1515  $\text{cm}^{-1}$ )<sup>88</sup>.

The amide III region of the spectra is important in inferring the protein's conformation, although usually the low signal/noise ratio makes it difficult to interpret spectra<sup>87</sup>. Pure FN is known to have amide III peaks at 1247, 1275, and 1290  $\text{cm}^{-1}$ <sup>88</sup>. These peaks have been reported to be different in FN adsorbed onto surfaces indicating that FN conformation is altered<sup>87</sup>. The peaks for the PCU-AA-FN in the amide III region were at 1310 (broad), 1265 (weak), and 1225  $\text{cm}^{-1}$  (broad) also suggesting FN conformation was different than the native form. Cooper et al. suggest that the shift of the 1247  $\text{cm}^{-1}$  peak to a lower frequency (such as seen 1225  $\text{cm}^{-1}$ ) still confirms the presence of the  $\beta$ -sheet structures as was also supported by the 1638  $\text{cm}^{-1}$  and 1680  $\text{cm}^{-1}$  bands found in the amide I region. This is not entirely unexpected, as circular dichroism studies on FN have indicated at most 15% of the secondary structure of FN is comprised of  $\alpha$ -helical structures, while 85% is estimated to be in anti-parallel  $\beta$ -form and unordered conformation<sup>89</sup>.

### 3.2 Toluidine Blue Assay

The TB assay made it possible to monitor the effect of increasing acrylic acid concentration and time of the grafting reaction on the number of introduced carboxylic acid groups in PCU-AA scaffolds. As toluidine blue complexes in a 1:1 ratio with carboxylic acid groups, the number of moles of toluidine blue extracted from scaffolds is equivalent to the number of carboxylic acid groups grafted on the scaffold. Furthermore, since a single molecule of AA contains a single COOH group, the quantification of moles of COOH groups grafted is equivalent to the moles of AA grafted. As seen in Figure 9, a calibration curve correlating known concentrations of toluidine blue and the absorbance read by a UV-Vis spectrophotometer at 633 nm was generated in order to interpolate results.

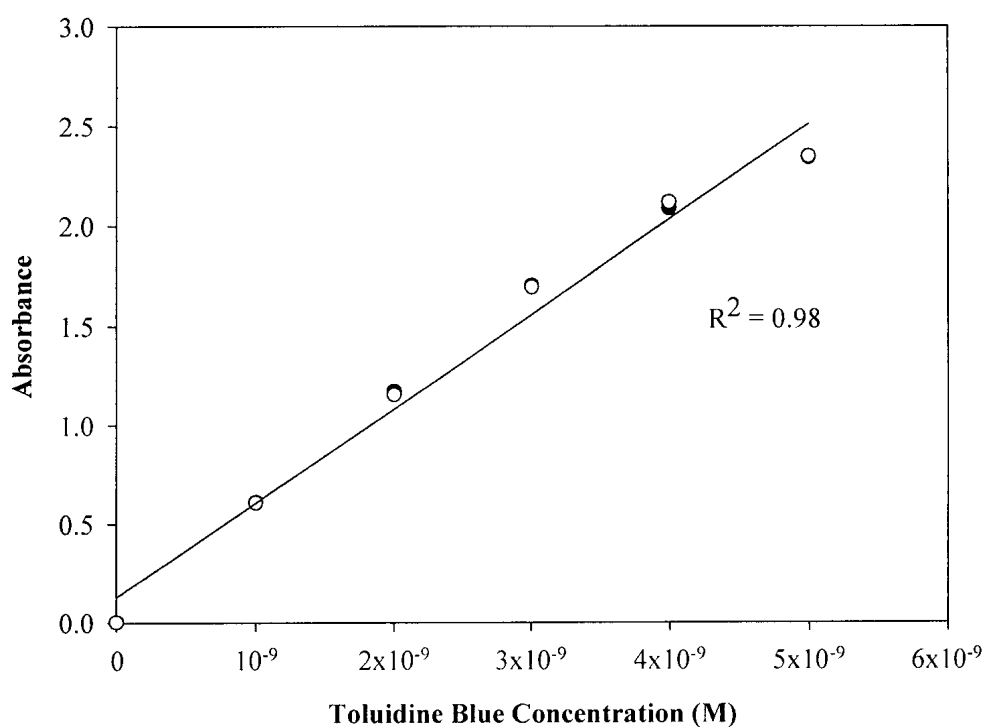


**Figure 9. A calibration curve correlating the absorbance read by a UV-Vis spectrometer at 633 nm and the concentration of toluidine blue in solution. The linear relationship was found to be: Absorbance = 47846 × Concentration + 0.1257.**

### 3.2.1. Effect of Time on the Moles of COOH Grafted

The effect of reaction time on the amount of acrylic acid groups grafted onto the 3D porous polyurethane scaffolds is presented in Figure 10. It can be seen that increasing AA grafting time increased the number of carboxylic acid groups grafted onto the PCU scaffolds. The moles of COOH groups increased by over a factor of 5 when the grafting time was increased from 30 min to 8 h using 6 M AA in the reaction.

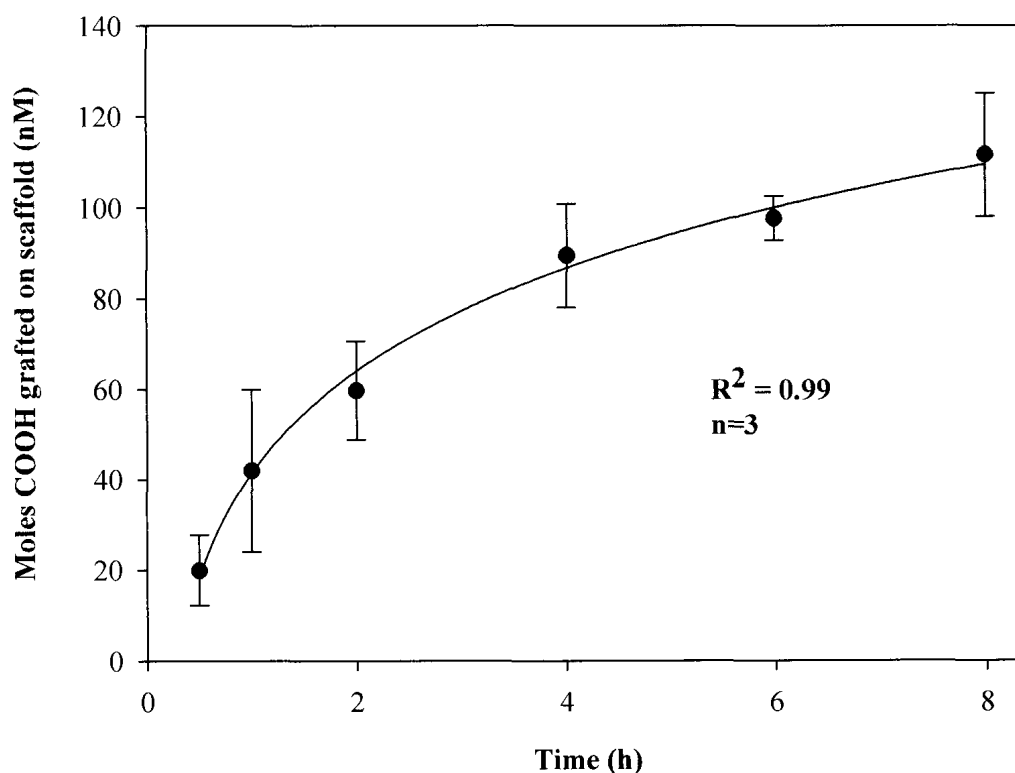


**Figure 10.** The effect of grafting time on the amount of COOH groups incorporated into the PCU scaffolds at a fixed concentration of 6 M acrylic acid.

The amount of COOH groups increased with time and the rate of COOH incorporation decreased with time. Data is presented as the mean  $\pm$  SD of experiments performed in triplicate.

At the earlier time points, the rate of acrylic acid grafted appeared to be higher than the latter time points (Figure 11). This observation is consistent with literature reports of ceric ion initiated polymerization, with the following possible explanations: (i) the rate of acrylic acid diffusion from the solution to the PCU scaffold reactive sites decreases as the polyacrylic acid (PAA) chain length increases with time, and, as the solution viscosity increases due to AA homopolymerization<sup>90,91</sup>; (ii) the AA monomer will eventually be depleted during the reaction or remain unreacted if the ceric (IV) ion is exhausted in the reaction mixture. These factors contribute to reduce the rate of AA grafted on the scaffolds with time. It should be stated that the PCU control scaffolds did not bind any toluidine blue.

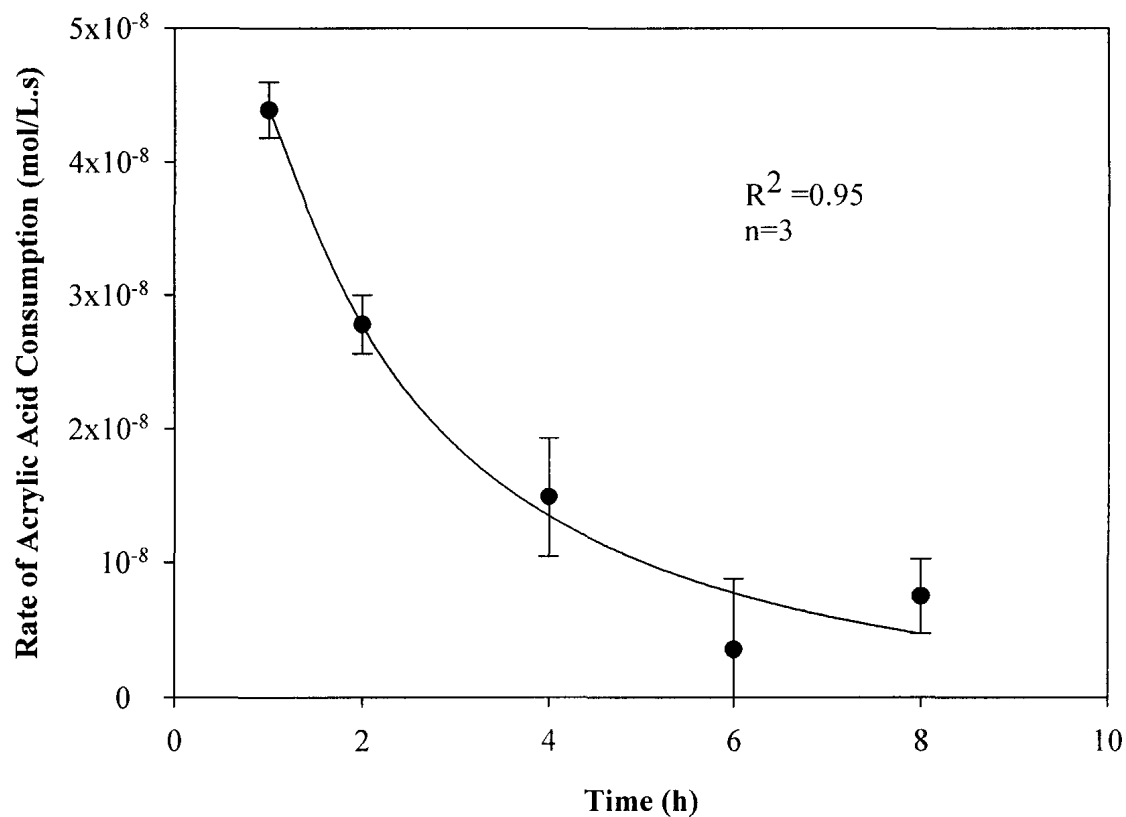


**Figure 11. The rate of moles of AA consumed in the grafting reaction as a function of time at 6M AA concentration.**

The initial rate of AA consumption is high but decreases rapidly to approach zero. The experimental rate at any given time is the change in the concentration of AA consumed per unit time.

### 3.2.2. Effect of Acrylic Acid Concentration on the Moles of COOH Grafted

The effect of AA concentration on COOH groups at a fixed reaction time of 1 h is presented in Figure 12. An increase of AA concentration from 1 M to 10 M increased the amount of COOH groups by a factor of 30. From a practical standpoint, AA concentrations beyond 6 M compromised scaffold porosity (please see Section 3.4). Thus, long reaction times at low AA concentrations are preferred to obtain useable scaffolds.

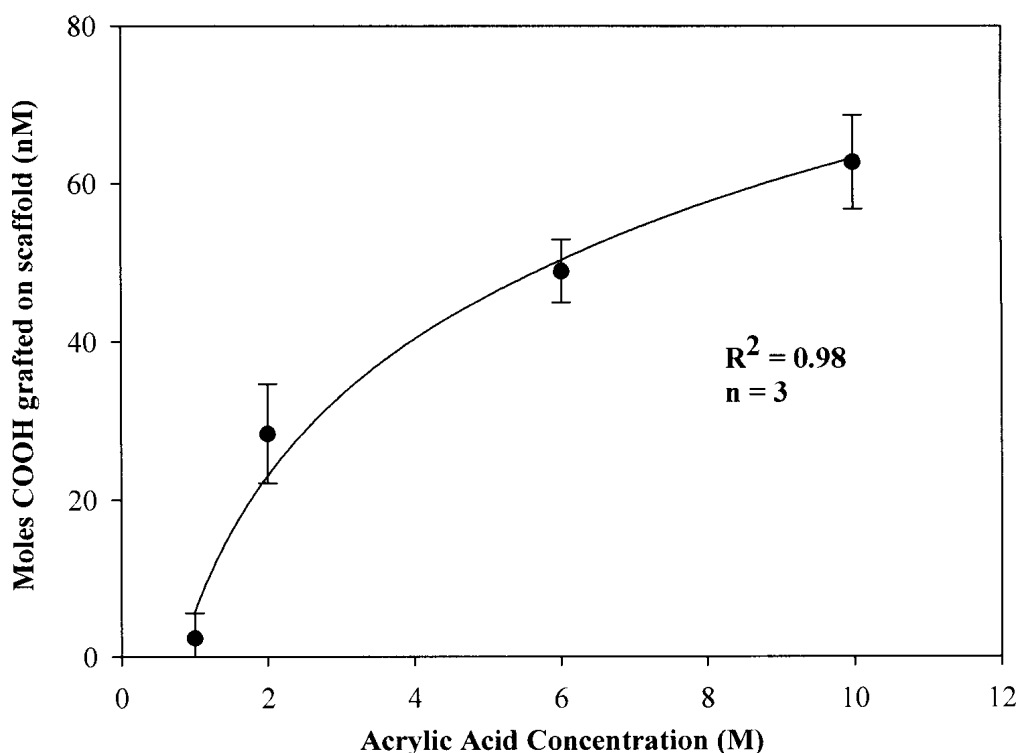


**Figure 12.** The effect AA concentration on the amount of COOH groups grafted onto PCU scaffolds for a fixed reaction time of 1 h.

The PCU control scaffolds did not bind any toluidine blue. Data is presented as the mean  $\pm$  SD of experiments performed in triplicate.

### 3.3 XPS Study of FN Conjugation to Scaffolds

#### 3.3.1. Survey Scans on Scaffolds

##### FN Conjugation onto 1 h, 6 M AA Grafted Scaffolds

XPS survey scans provided the atomic compositions of PCU, PCU-AA, PCU-AA-NHS, and PCU-AA-FN scaffolds. Table 2 summarizes these results for scaffolds for 1 h AA grafted scaffolds.

**Table 2. The atomic composition of PCU, PCU-AA, and PCU-AA-FN scaffolds as determined by XPS survey scans for 1 h, 6 M AA grafts.**

Scaffold	Atomic Percentage (%)				Ratios	
	C <sub>1s</sub>	N <sub>1s</sub>	O <sub>1s</sub>	S <sub>2p</sub>	(N/C)	(O/C)
PCU	75.6	3.4	21.0	0.0	0.04	0.28
PCU-AA	76.0	0.7	23.3	0.0	0.01	0.31
PCU-AA-NHS	68.8	10.4	20.8	0.0	0.15	0.30
PCU-AA-FN (0.1 mg FN)	68.0	4.6	27.3	0.0	0.07	0.40
PCU-AA-FN (0.2 mg FN)	69.1	7.2	23.0	0.3	0.10	0.33
PCU-AA-FN (0.5 mg FN)	67.2	11.5	20.7	0.6	0.17	0.31
PCU-AA + 0.5 mg FN <sup>(a)</sup>	73.0	3.2	23.6	0.2	0.04	0.32

(a) Serves as a FN adsorption control.

Due to the intrinsic high carbon and oxygen contents in the scaffolds, changes in C and O composition upon AA grafting and FN conjugation were not drastic. Changes in atomic nitrogen, however, were apparent, and can be attributed to two principle reasons: first, the N<sub>1s</sub> level in the PCU is only 3.4% of the entire polymer (derived from the urethane

moiety) and second, FN is a large 500 kDa protein rich in nitrogen derived from its polypeptide backbone.

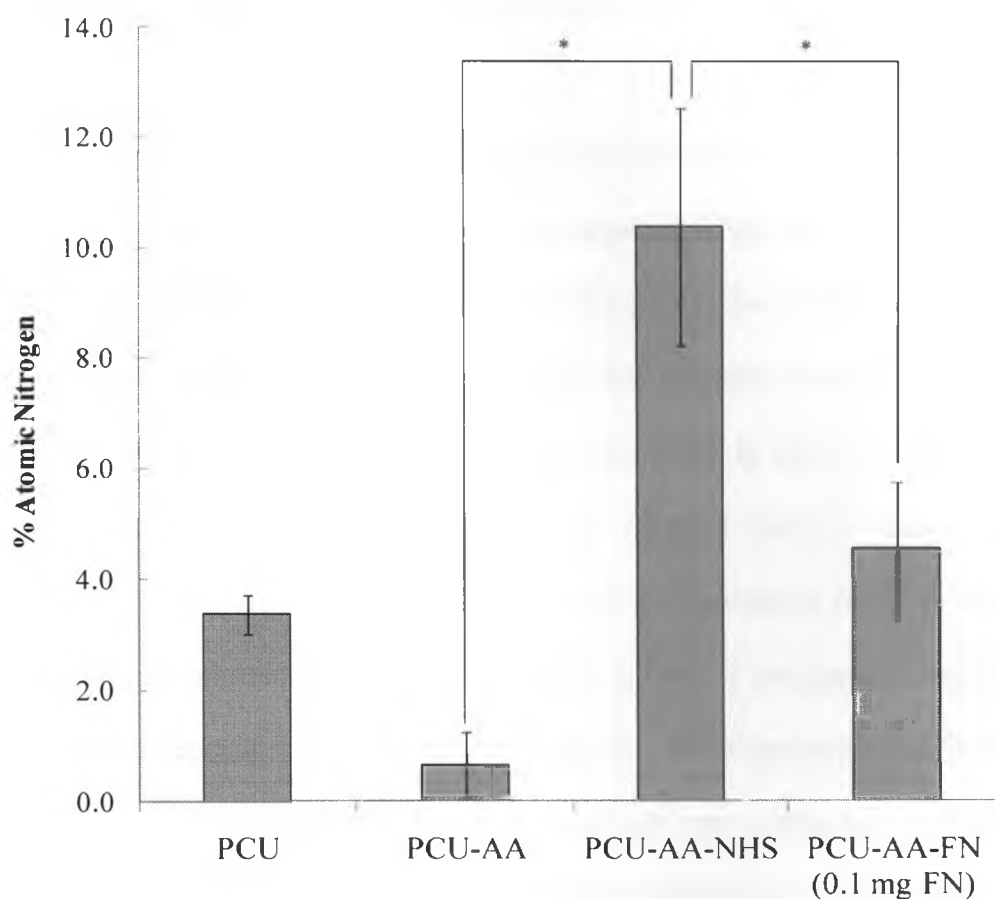


**Figure 13. XPS analysis of N1s levels for PCU, PCU-AA, PCU-AA-NHS and PCU-AA-FN scaffolds.**

6M AA is used for these experiments. Nitrogen levels are reduced to near 0 in the PCU-AA as PAA grafts onto the urethane nitrogen but are elevated in PCU-AA-NHS scaffolds due to the nitrogen in NHS. Nitrogen in PCU-AA-FN scaffolds reflects the protein content (immobilized and absorbed). Results are expressed as the mean of three samples  $\pm$  SD. Statistical analysis was performed using the one-tailed unpaired Student t-test (\* $p < 0.05$ ).

As shown in Figure 13, the PCU control scaffolds contained  $3.4 \pm 0.4\%$  nitrogen. Following AA grafting,  $N_{1s}$  in these scaffolds was  $0.7 \pm 0.6\%$  indicating that the majority of the urethane nitrogen were covered by grafted PAA chains. Activated PCU-AA-NHS

scaffolds showed a high level of  $N_{1s}$ , which is derived from NHS. In order to verify that there was no reaction between the PCU scaffolds and the activation solution, as a control, PCU scaffolds were exposed to the EDC/NHS solution and the  $N_{1s}$  level was 2.1%.

It is unlikely that any unreacted NHS-ester will be present after 24 h of the conjugation reaction since its half-life is between 2 to 4 h in aqueous environments<sup>86</sup>. This expectation was further supported by the loss of the succinimidyl ester in the FT-IR spectra of PCU-AA-FN scaffolds. Thus it was anticipated that the nitrogen content after the FN conjugation reaction would be reflective of immobilized FN. In order to investigate the effect of FN concentration on the amount of nitrogen present, three different concentrations of FN were examined at a fixed conjugation time of 24 h. As shown in Figure 14, nitrogen substantially increased, suggesting that the conjugation reaction was FN concentration dependent. At the same time, the N/C ratios increased with increasing FN concentration. FN adsorption on PCU-AA scaffolds was evaluated by omitting the NHS/EDC activation step and immersing the scaffolds in the highest concentration of FN used in actual conjugation reactions. As seen in Figure 14 and Table 2, the nitrogen content in FN-conjugated scaffolds was 3.6 times greater than that of FN-adsorbed scaffolds. Thus, FN adsorption on scaffolds does not supersede the effectiveness of FN conjugation.

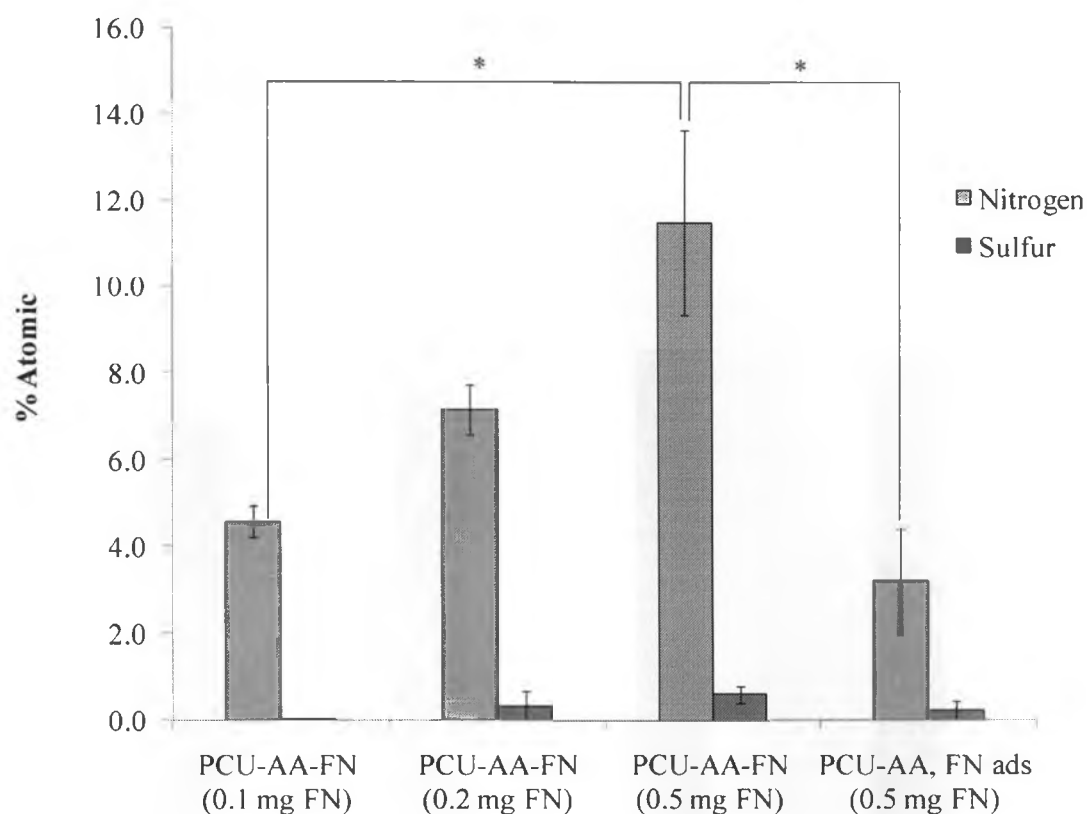


**Figure 14. XPS analysis on  $N_{1s}$  and  $S_{2p}$  for FN immobilized scaffolds on 1 h 6 M AA grafts for 24 h.**

Nitrogen levels increase with increasing FN concentrations used in the conjugation solution. The maximum possible FN adsorbed is significantly lower than immobilized (3.2% vs 11.5%). Results are expressed as the mean of three samples  $\pm$  SD. Statistical analysis was performed using the one-tailed unpaired Student t-test (\* $p < 0.05$ ).

Sulfur, derived from the disulfide linkages due to cysteine oxidation in the protein, was detected for the higher concentration of fibronectin conjugated scaffolds at a binding energy of 163 eV. There are roughly 62 cysteine residues per subunit of fibronectin, representing a total of 3% (mol) in the entire 500 kDa protein<sup>74</sup>. For 1 h 6M AA grafts, the sulfur content increased with an increase of the fibronectin in the conjugation solution. The data for Figure 13 was based on 24 h conjugation time. In order to investigate the effect of conjugation time on the nitrogen composition of scaffolds,

conjugation reactions were also performed for 1, 6, and 12 h using 0.5 mg FN. The results are presented in Figure 15.

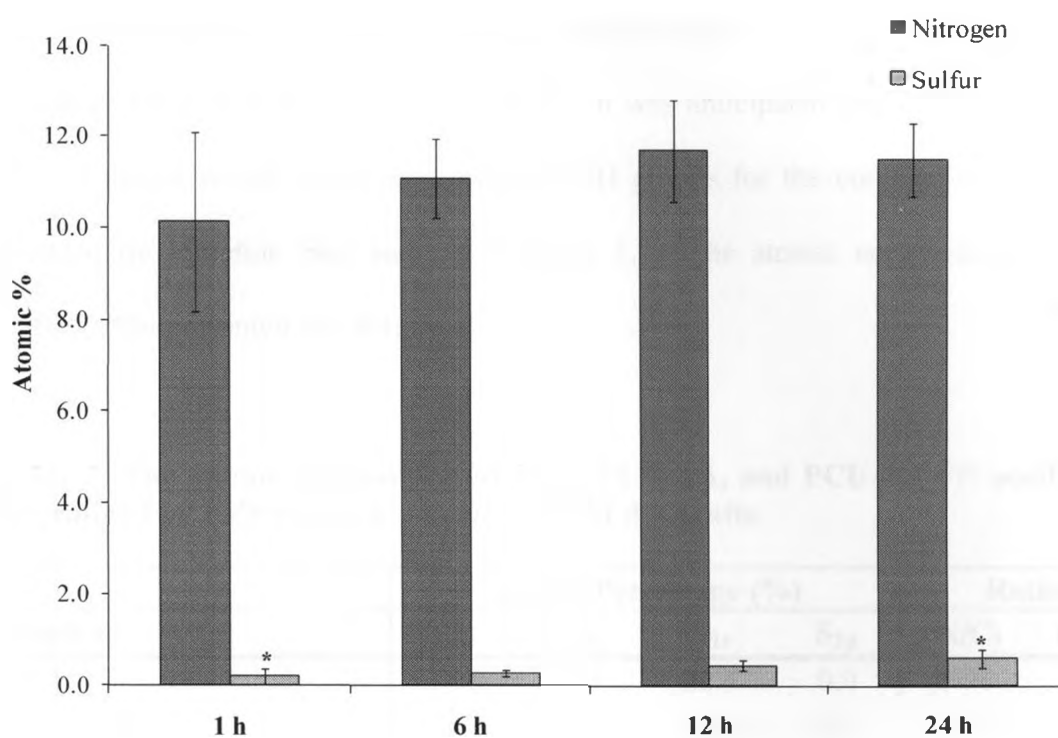


**Figure 15. XPS analysis on the effect of FN conjugation time on the atomic %  $N_{1s}$  and  $S_{2p}$  using 0.5 mg FN.**

It appears that there is no significant change in nitrogen content, and hence, the extent of FN conjugated between 1 h to 24 h. There is a significant difference in the sulfur content between 1 h and 24 h FN conjugation times. Results are expressed as the mean of three samples  $\pm$  SD. Statistical analysis was performed using the one-tailed unpaired Student t-test (\* $p < 0.05$ ).

In FN-conjugated scaffolds, there was no statistical difference in nitrogen composition between 1, 6, 12, and 24 h conjugation reaction times ( $p > 0.05$ ). However, the sulfur content was significantly different between 1 h and 24 h reaction times ( $p < 0.05$ ). As aforementioned, an NHS ester has an expected half-life of 2-3 h at room temperature. Therefore, it is likely some unreacted NHS-ester may contribute to some of the nitrogen present at the earlier time points, i.e., 1 h.

### FN Conjugation on 6 h, 6M AA Grafted Scaffolds

In order to investigate the effects of FN conjugation on scaffolds that are AA grafted for longer times than 1 h, PCU-AA scaffolds were generated at 6 h AA grafting times using the same AA concentration as before (6 M). It was anticipated that the 6 h AA grafted PCU scaffolds would encompass more COOH groups for the conjugation reaction, as revealed by toluidine blue staining (Section 3.2). The atomic compositions of these scaffolds are presented in Table 3.

**Table 3. The atomic composition of PCU, PCU-AA, and PCU-AA-FN scaffolds as determined by XPS survey scans for 6 h, 6 M AA grafts.**

Scaffold	Atomic Percentage (%)				Ratios	
	C <sub>1s</sub>	N <sub>1s</sub>	O <sub>1s</sub>	S <sub>2p</sub>	(N/C)	(O/C)
PCU	74.5	3.1	22.4	0.0	0.04	0.30
PCU-AA	73.7	0.0	26.4	0.0	0.00	0.36
PCU-AA-FN (0.2 mg FN)	65.2	10.4	24.0	0.5	0.16	0.37
PCU-AA-FN (0.5 mg FN)	65.8	13.1	20.6	0.3	0.20	0.31
PCU-AA + 0.5 mg FN <sup>(a)</sup>	66.7	11.7	21.3	0.2	0.18	0.32

(a) Serves as a FN adsorption control.

As seen in Table 3, the O<sub>1s</sub> content for PCU-AA scaffolds is 26.4%, which is 3.1% higher than PCU-AA scaffolds grafted for 1 h (Table 2), and reflects the increased amount of COOH groups incorporated for longer grafting times. As expected, no nitrogen was detected in these PCU-AA scaffolds. The nitrogen levels for these PCU-AA-FN scaffolds grafts were higher than levels detected on the corresponding PCU-AA-FN scaffolds using 1 h AA grafts (Figure 16). Furthermore, the contribution of nitrogen levels from FN adsorbed on these PCU-AA scaffolds was significantly large, especially

in comparison to that detected for PCU-AA-FN conjugated scaffolds using the same FN concentration.

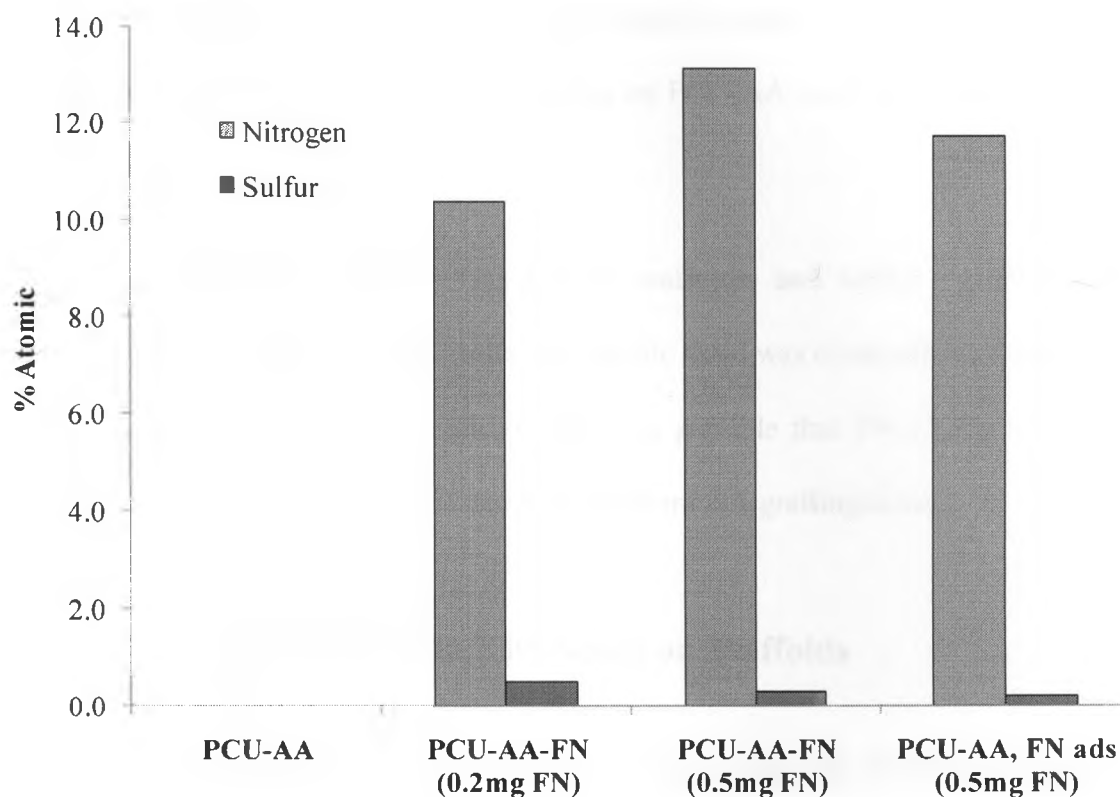


**Figure 16.** XPS analysis on  $N_{1s}$  and  $S_{2p}$  for FN immobilized on 6 h 6M AA grafts. Nitrogen levels increase with increasing FN concentration used in the conjugating solution. The nitrogen contribution from FN adsorption is comparable to that conjugated.

The possible explanation for this is an increased electrostatic attraction for higher grafted COOH concentrations; Since fibronectin has an isoelectric point at pH 5.2<sup>92</sup>, it is positively charged in the MES buffer (pH 4.1) as the amino groups are protonated ( $NH_3^+$  form). Furthermore, at pH 4.1, the degree of ionization of PAA is 0.2<sup>93</sup> and PCU-AA scaffolds will have a slightly negatively charged surface, promoting the electrostatic adsorption of FN. As revealed by toluidine blue staining, there are 2.5 times more PAA

chains for the 6 h AA grafts compared to the 1 h, and thus electrostatic adsorption of FN is greater on 6 h AA grafted scaffolds. Similar observations have been reported for the interaction between PAA and proteins<sup>94</sup>. Since FN adsorption appears to be dominant on PCU-AA scaffolds containing a higher COOH grafting density than FN conjugation, it is preferable to perform FN conjugation studies on PCU-AA scaffolds grafted for shorter reaction times.

Sulfur was detected on these PCU-AA-FN scaffolds, and unlike the PCU-AA-FN scaffolds generated from 1 h AA grafts, no specific trend was observed. Perhaps cysteine exposure is FN conformation sensitive, and it is possible that FN conformation varies when immobilized on scaffolds treated with different AA grafting times.

### **3.3.2. High Resolution XPS Scans on Scaffolds**

The XPS survey scan discussed in the previous sections provide little information on the functional groups present at the different conjugation steps. Therefore, a high resolution XPS scan for PCU, PCU-AA, and PCU-AA-FN scaffolds were conducted. Since 1 h AA grafting with a 6 M solution followed by 24 h FN conjugation presented the most representative samples, high resolution XPS scans were performed on these scaffolds. The resulting data can confirm changes in chemical bond types associated with each of the intermediates. There are several other high resolution XPS studies performed on FN modified polymer substrates (films)<sup>67, 95-96</sup>. In each of these reports the N<sub>1s</sub> signal was used as a marker for peptide modification, as was assumed in this study. Table 4 and

Table 5 summarize these findings, and these are followed by detailed descriptions of the bond assignments.

**Table 4. High resolution XPS C1s scan results for PCU, PCU-AA, and PCU-AA-FN scaffolds. Values represent the percent associated to each bond type. Note that (-) denotes 0%.**

	C1s Binding Energies (eV)					
	285.0	286.7	288.1	288.9	289.4	290.4
	<u>C-C</u> , <u>C-H</u>	<u>C-O-C</u>	<u>O=C-N</u>	<u>O-C=O</u>	<u>N-(C=O)-O</u>	<u>O-(C=O)-O</u>
PCU	69.7	22.4	-	-	1.9	6.1
PCU-AA	73.1	14.9	-	12.0	-	-
PCU-AA-FN	51.4	28.2	18.3	-	-	2.1

**Table 5. High resolution XPS N1s and O1s scan results for PCU, PCU-AA, and PCU-AA-FN scaffolds. Values represent the percent associated to each bond type. Note that (-) denotes 0%.**

	N1s Binding Energies (eV)		O1s Binding Energies (eV)		
	400.3	401.7	531.6	532.0	533.7
	<u>H-N-(C=O)-O</u> , <u>N-(C=O)</u>	<u>N-H<sub>2</sub></u> , <u>N-H<sub>3</sub><sup>+</sup></u>	<u>C=O-N</u>	<u>C=O-O</u>	<u>C-O-C</u>
PCU	100.0	-	-	35.9	64.1
PCU-AA	-	-	-	72.2	27.8
PCU-AA-FN	88.9	11.1	59.8	-	40.2

### N<sub>1s</sub> Spectra

Figure 17 shows the N<sub>1s</sub> signals found for PCU, PCU-AA, and PCU-AA-FN. This is one of the simpler spectra to describe. The urethane nitrogen (H-N-(C=O)-O), at 400.3 eV, represents 100% of N<sub>1s</sub> spectra for PCU scaffolds. This is in agreement with the literature, as the nitrogen peak from the isocyanate contribution in the polyurethane structure is known to arise around 400.5 eV<sup>97</sup>. Recalling that N<sub>1s</sub> detection was nearly 0% in survey scans of PCU-AA scaffolds, high resolution spectra confirmed the same result. In the PCU-AA-FN scaffolds, two peaks emerged at 400.3 eV and 401.7 eV. The peak representing the amide nitrogen (N-(C=O)) appeared exactly as expected for a typical amide bond,  $400.3 \pm 0.1$  eV<sup>95</sup>, and represented most of the form of nitrogen (88.9%). The remaining 11.1% nitrogen appeared as free amine content associated with FN and is also consistent with literature reports of the peak at 401.7 eV<sup>98</sup>. Note that the free amine groups in FN can either arise from the N-terminus of the protein, as well as amino acids that contain amines in their side chain such as lysine, arginine and glutamine.

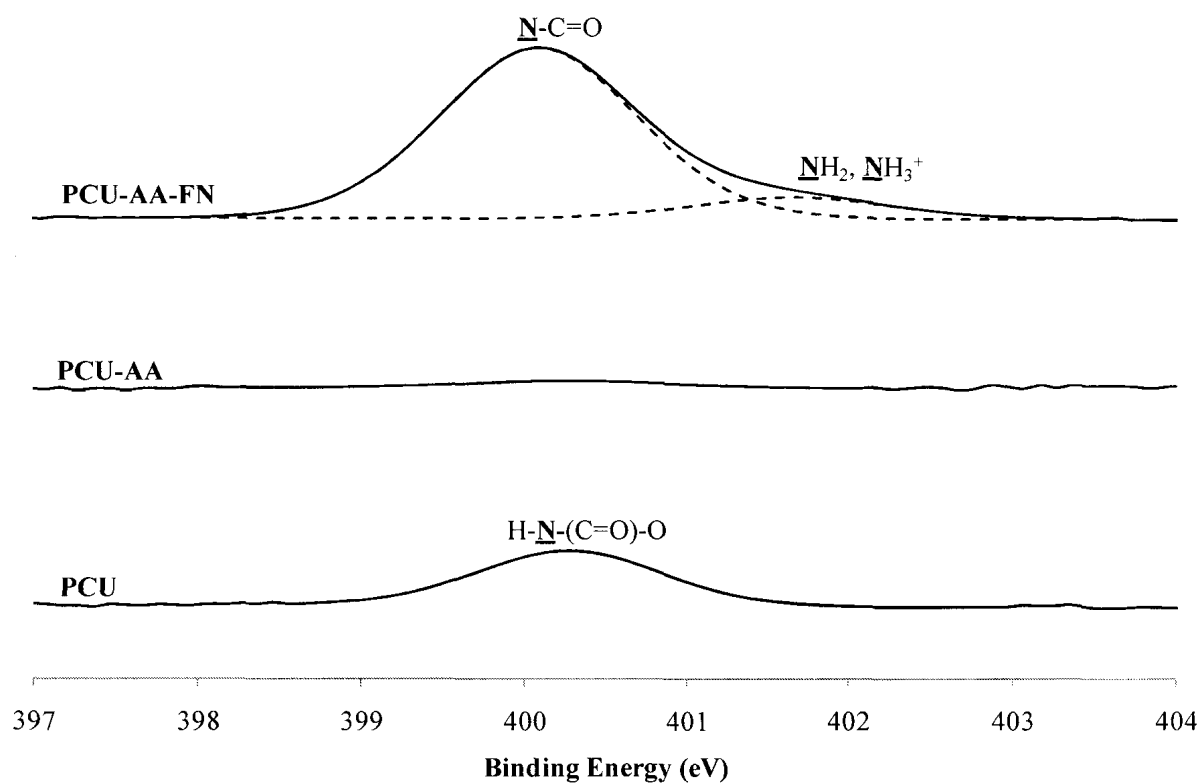


**Figure 17. High resolution XPS  $N_{1s}$  spectra of PCU, PCU-AA, and PCU-AA-FN scaffolds showing peak integrations.**

The single peak in the PCU represents the urethane nitrogen. Upon AA grafting, the nitrogen is buried AA groups and is not detected. The PCU-AA-FN scaffolds exhibit two types of nitrogen peaks, the larger one arising from the amide bond and the smaller one from free amine groups associated with FN. The solid line represents the overall element integration while the dashed lines represent integrations of distinct binding energies.

### C1s Spectra

As presented in Figure 18, the four distinct binding energies at 285.0, 286.7, 289.4, and 290.4 eV for PCU scaffolds are assigned to the alkyl ( $\underline{\text{C}}\text{-C}$ ,  $\underline{\text{C}}\text{-H}$ ), ether ( $\underline{\text{C}}\text{-O-C}$ ), urethane ( $\text{N-}(\underline{\text{C}}=\text{O})\text{-O}$ ) and carbonate ( $\text{O-}(\underline{\text{C}}=\text{O})\text{-O}$ ) groups respectively<sup>99</sup>. Carbon is predominantly in the form of alkyl and ether groups totaling 92.1%, while the urethane moiety represents only 1.9% of the carbon spectra. A new binding energy at 288.9eV appears for the PCU-AA sample and is assigned to the ( $\text{O-}\underline{\text{C}}=\text{O}$ ) carboxylic acid groups from grafted PAA<sup>100</sup>, representing 12% of the carbon spectra. At the same time, the urethane carbon in PCU-AA scaffolds is diminished to 0%. This is consistent with the elemental data for nitrogen, which is almost reduced to 0% of the overall atomic composition upon AA grafting.

In the PCU-AA-FN sample, the expected amide functionality ( $\text{O=}\underline{\text{C}}\text{-N}$ ) is introduced at 288.1eV<sup>98</sup>, while that of the ( $\text{O-}\underline{\text{C}}=\text{O}$ ) is reduced to 0, confirming the conjugation reaction. Note that in these samples, the carbon associated with the amide form is 18.3% of the total carbon and is the largest non-alkyl/ether contribution in comparison to all of the other scaffolds (PCU, PCU-AA).

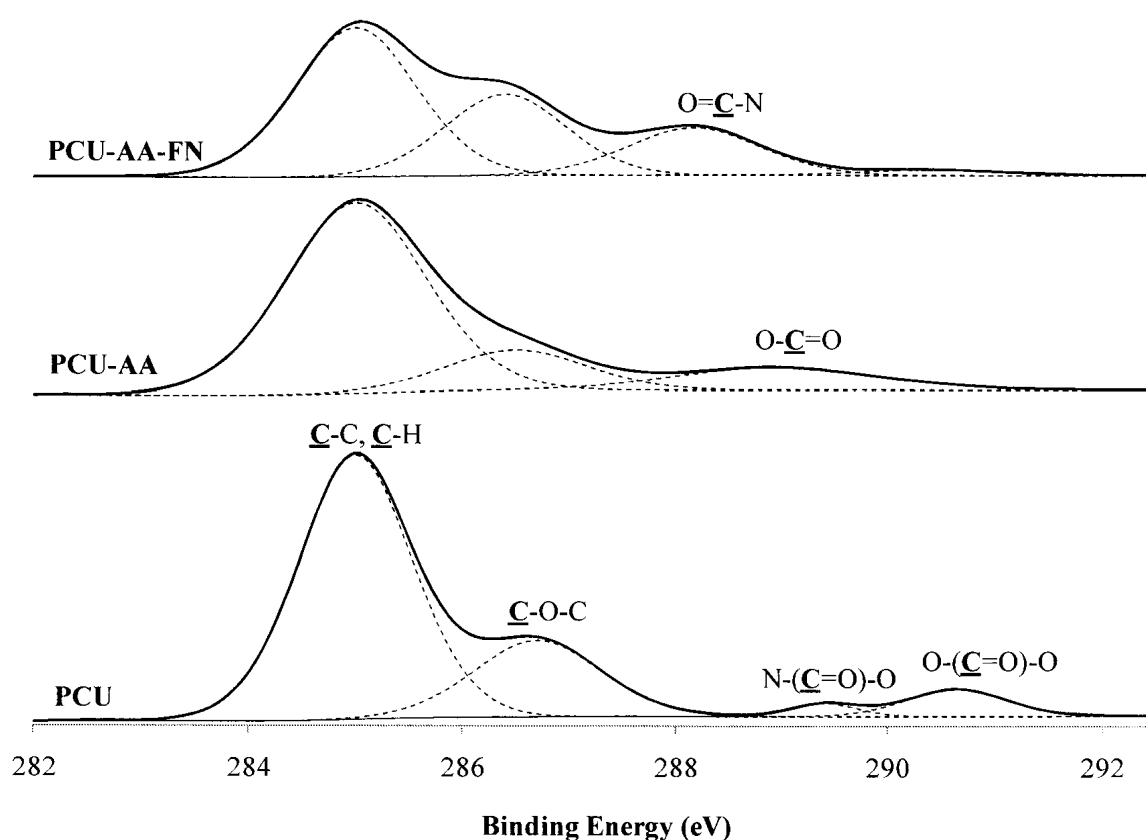


**Figure 18. High resolution XPS  $C_{1s}$  spectra of PCU, PCU-AA, and PCU-AA-FN scaffolds showing peak integrations.**

The binding energy for the urethane carbon is visible only in PCU scaffolds. The binding energy for the carbon of carboxylic acids appears in PCU-AA scaffolds, while that of the amide group appears in PCU-AA-FN scaffolds. The solid line represents the overall element integration while the dashed lines represent integrations of distinct binding energies.

In the PCU-AA-FN sample, the expected amide functionality ( $O=\underline{C}-N$ ) is introduced at 288.1 eV<sup>98</sup>, while that of the ( $O-\underline{C}=O$ ) is reduced to 0, confirming the conjugation reaction. Note that the urethane moiety represents only 1.9% of the carbon spectra, and is diminished to 0% upon AA grafting. This is consistent with the elemental data for nitrogen, which is effectively 0% of the overall atomic composition upon AA grafting.

### O1s Spectra

The PCU scaffolds had two characteristic peaks at 532.0 eV and 533.7 eV (Table 4), attributed to the oxygen of the urethane ester ( $\text{C}=\underline{\text{O}}\text{-O}$ ) and ether linkage ( $\text{C}-\underline{\text{O}}\text{-C}$ )<sup>101</sup>. Since a large amount of oxygen was contributed from the grafted AA groups, the percentage of  $\text{C}=\underline{\text{O}}\text{-O}$  groups in PCU-AA scaffolds were found to be double than that of the PCU scaffolds. Upon FN conjugation, the PCU-AA-FN reveal that almost 60% of the oxygen is in the amide form ( $\text{C}=\underline{\text{O}}\text{-N}$ )<sup>98</sup>. Figure 19 provides a detailed visual of these descriptions.

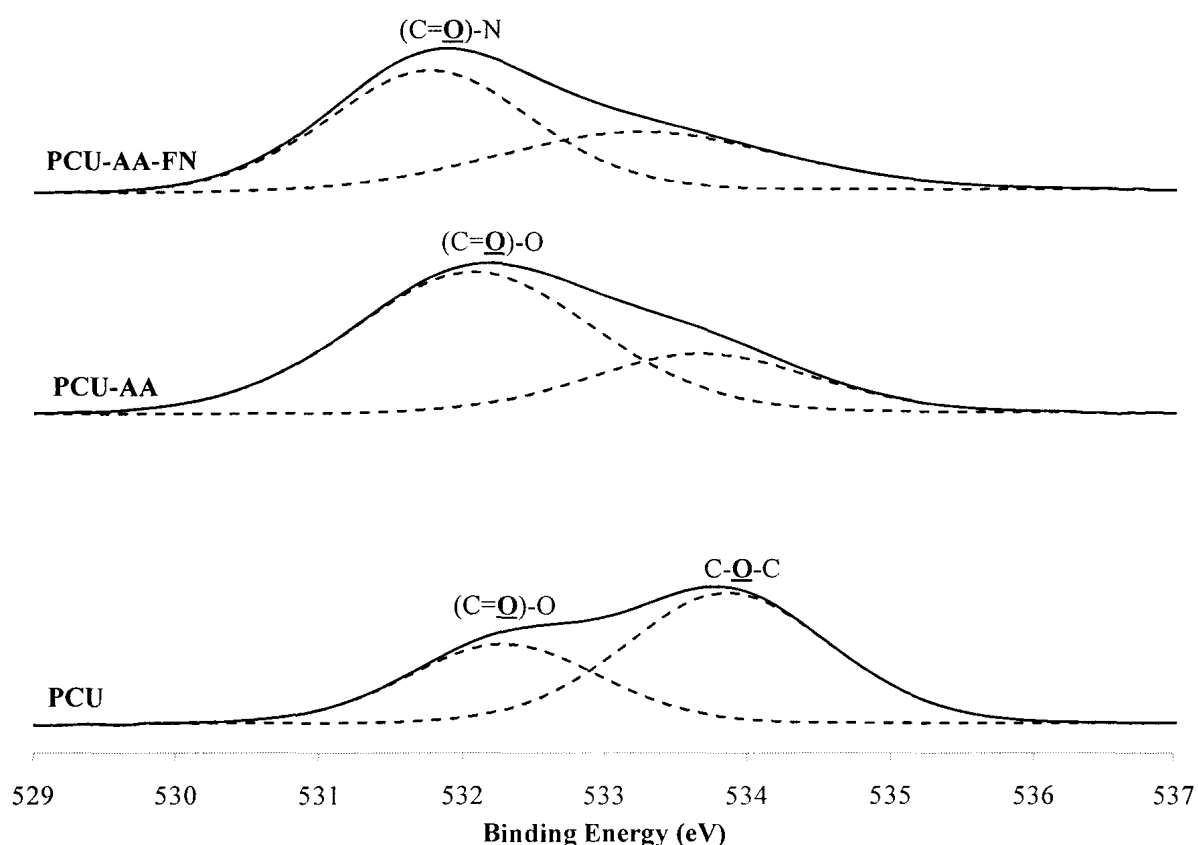


**Figure 19. High resolution XPS O<sub>1s</sub> spectra of PCU, PCU-AA, and PCU-AA-FN scaffolds showing peak integrations.**

In the PCU scaffolds, the ether linkage is most prominent. PCU-AA scaffolds have a marked increase in the  $\text{C}=\underline{\text{O}}\text{-O}$  peak, attributed to the grafted carboxylic acid groups in PAA. A new binding energy representing the oxygen associated with amide bonds arises

### 3.4 SEM Observation of Scaffolds

For 3D scaffolds intended for tissue engineering applications, it is important that the grafting and subsequent conjugation reactions do not interfere with their porosity and pore interconnectivity. Thus, SEM images of scaffolds were taken before and after various chemical treatments in order to verify the maintenance of porous structure and integrity (Figure 20). For AA concentrations up to 6 M, increasing the grafting time did not compromise the porous structure of the scaffolds (Figure 20C, D), although moderate scaffold swelling was apparent for longer reaction times when placed in water. Beyond 6 M, increasing AA concentration increased scaffold swelling in water, and in the extreme case of 18 M, the scaffold pores became ill-defined and the pore geometries were distorted (Figure 20E). The reason for this could be due to increased grafted AA and also some AA homopolymerization that potentially clogged the pores of the scaffolds. For PCU-AA-FN scaffolds prepared following 6 M AA concentration in the grafting solution, the porosity and pore interconnectivity were preserved (Figure 20F) and no apparent difference was observed when compared with PCU control scaffolds (Figure 20A, B).

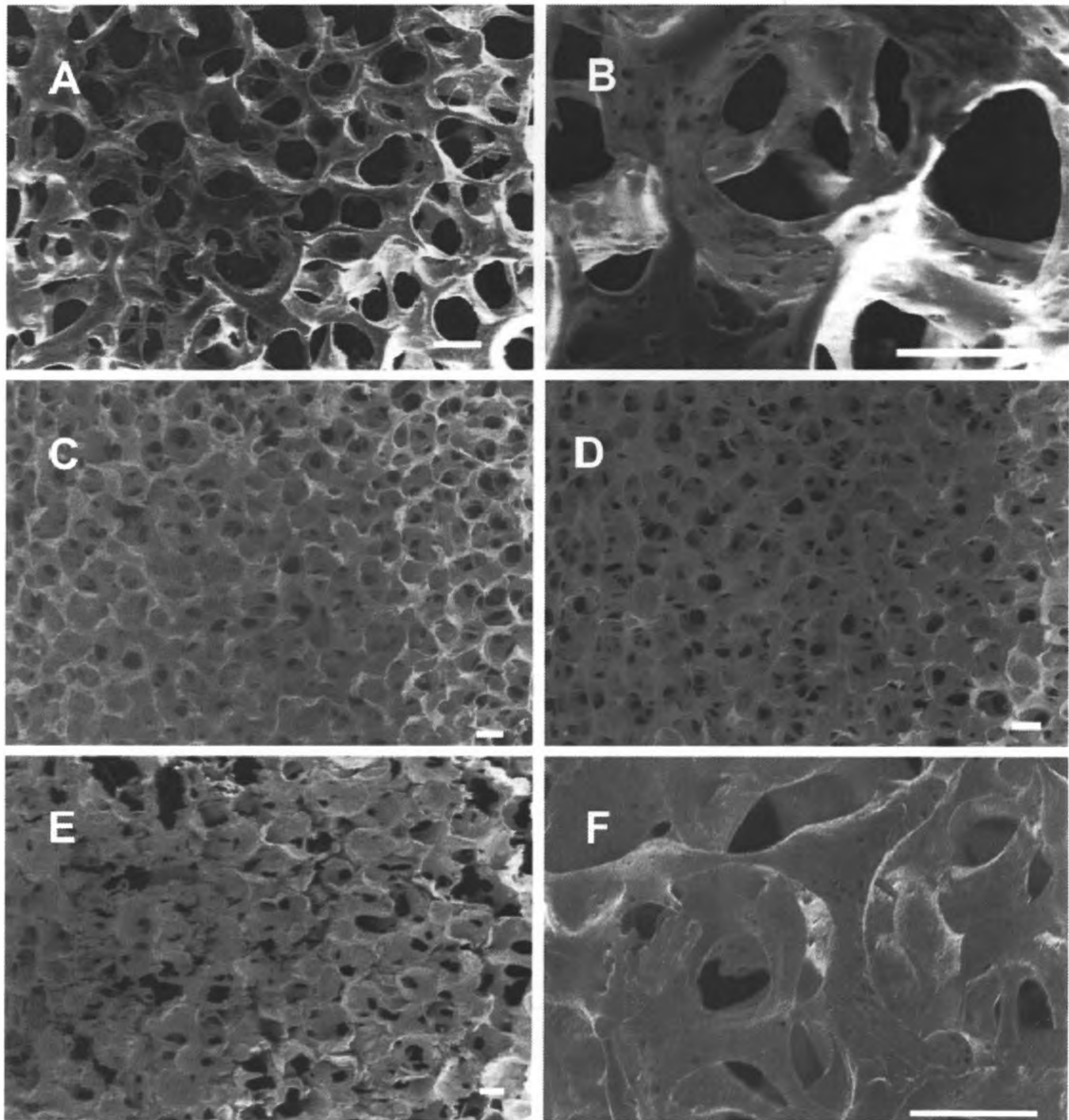


**Figure 20. Scanning electron micrographs of PCU scaffolds.**

(A) unmodified PCU; (B) close-up of pore structure in unmodified PCU; (C) 6 M acrylic acid grafted for 1 h; (D) 6 M acrylic acid grafted for 8 h; (E) 18 M acrylic acid grafted for 1 h; (F) 6 M acrylic acid grafted for 1 h and 0.5 mg FN immobilized. Scaffold geometry was maintained except for high acrylic acid concentrations (E). Scale bar represents 100  $\mu\text{m}$ .

### **3.5 FN Leaching Study Using the BCA Assay**

Tissue engineering scaffolds are processed in the presence of fluids before cell seeding. This includes ethanol sterilization followed by PBS rinsing, preconditioning with HBSS or with similar buffers. In all these steps, the conformation of either the conjugated or the adsorbed FN may be altered. In addition, the adsorbed FN presented in Figure 14 may not survive these processing conditions. We therefore investigated to what extent the adsorbed or conjugated FN is affected by PBS leaching and in the most aggressive case using SDS for accelerated leaching over time. The BCA Assay was used to quantify FN concentrations in each of the PBS and SDS solutions. A calibration curve correlating known FN concentrations in PBS and the absorbance is presented in Figure 21. The results of the leaching study are presented in Figure 22.

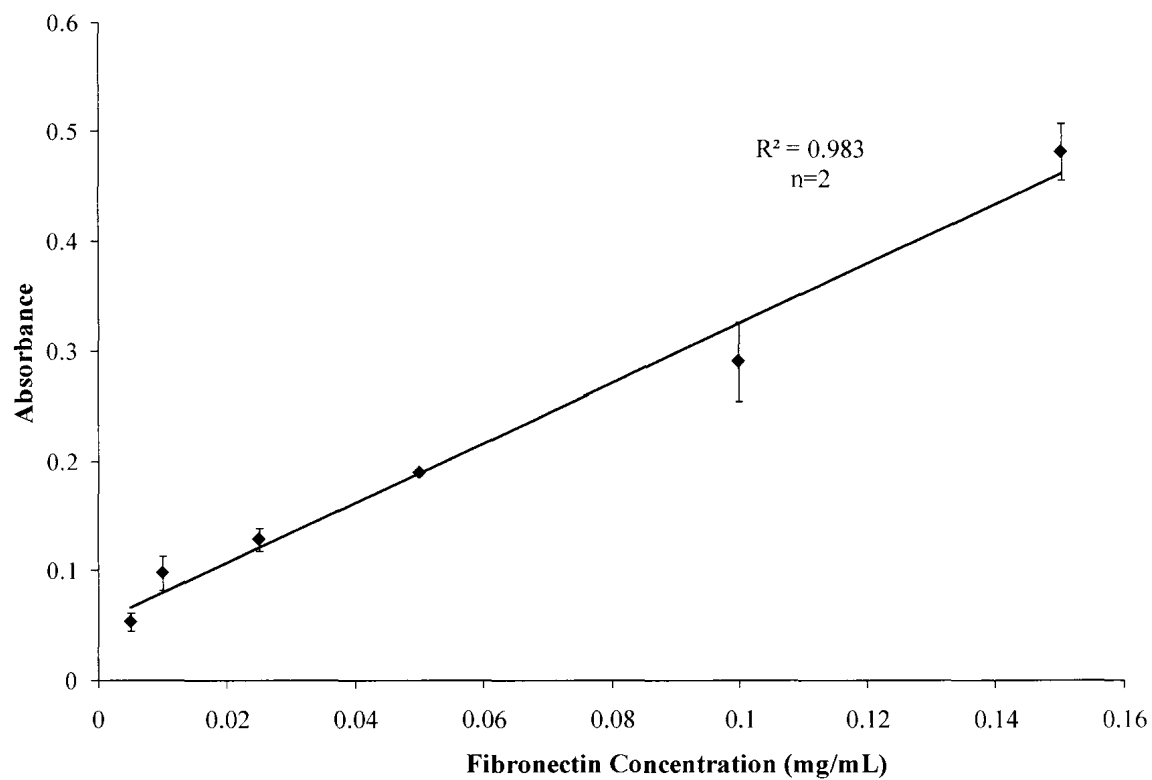


**Figure 21.** A calibration curve for the BCA assay correlating the concentration of FN in solution with the absorbance read at 562 nm with a UV-Vis spectrophotometer.

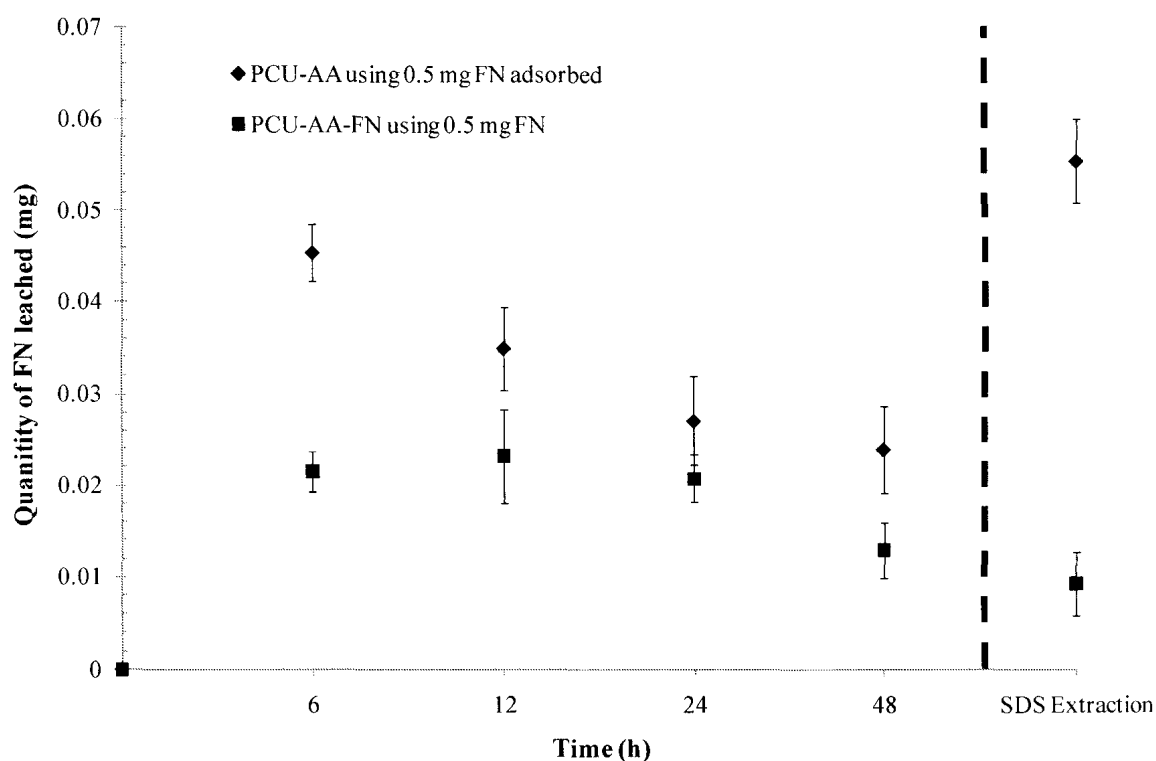


**Figure 22. Quantities of FN leached with time from PCU-AA-FN (0.5 mg FN) and PCU-AA FN adsorbed (0.5 mg FN) scaffolds.**

PCU-AA FN adsorbed scaffolds lost more FN than PCU-AA-FN scaffolds. Little FN was retrieved from PCU-AA-FN scaffolds after 24 h. The PCU-AA FN adsorbed scaffolds lost the most FN upon SDS leaching. Results are expressed as the mean of three samples  $\pm$  SD.

For PCU-AA scaffolds with 0.5 mg FN adsorbed, it appears that the amount of FN leached per time period decreases. After 24 h, more than 0.1 mg of FN has been leached. The SDS extraction removed a large quantity of FN adsorbed FN on these scaffolds. The remainder of adsorbed FN was likely trapped in pores and difficult to leach under static conditions. A total of 0.18 mg of FN was recovered from the FN adsorbed scaffolds. The remaining FN was either washed during initial PBS rinses or adsorbed onto the glass vial used to prepare the sample.

For the PCU-AA-FN scaffolds, it appears that beyond 24 h, there is a small amount of adsorbed FN that can be leached. Also, very little FN was detected in the SDS extraction. A total of 0.09 mg of FN was retrieved from these PCU-AA-FN scaffolds, indicating the FN adsorbed scaffolds did indeed lose more FN. Here, the remaining FN was either washed during initial PBS rinses, adsorbed onto the glass vial used to prepare the sample, or conjugated on the scaffold.

### **3.6 Immunofluorescence Study of FN on Various Scaffolds**

Immunofluorescence studies were conducted in order to visually identify the presence of FN on PCU-AA-FN scaffolds before and after SDS leaching, and the results are presented in Figure 23. The secondary antibody used in this study was Texas-Red conjugated as PCU auto-fluoresces in the green wavelength. The control used in this study was a PCU-AA scaffold, which did not fluoresce after incubation with primary and secondary antibodies for FN (Figure A). The PCU-AA scaffold exposed to 0.5 mg of FN showed some fluorescence (Figure 23B), while certain regions did not stain positively at all. This fluorescence was expected and attributed to FN adsorption onto the scaffold surfaces due to the electrostatic interactions between the positively charged protein and negatively charged acrylic acid groups at the experimental pH (4.2). The PCU-AA-FN scaffolds prepared using 0.5 mg FN in the conjugation reactions showed an intense fluorescence in the red wavelength after antibody staining (Figure C). The FN appeared to be distributed evenly over the scaffold surfaces such that the pores of the scaffold were outlined by the secondary antibody stain.

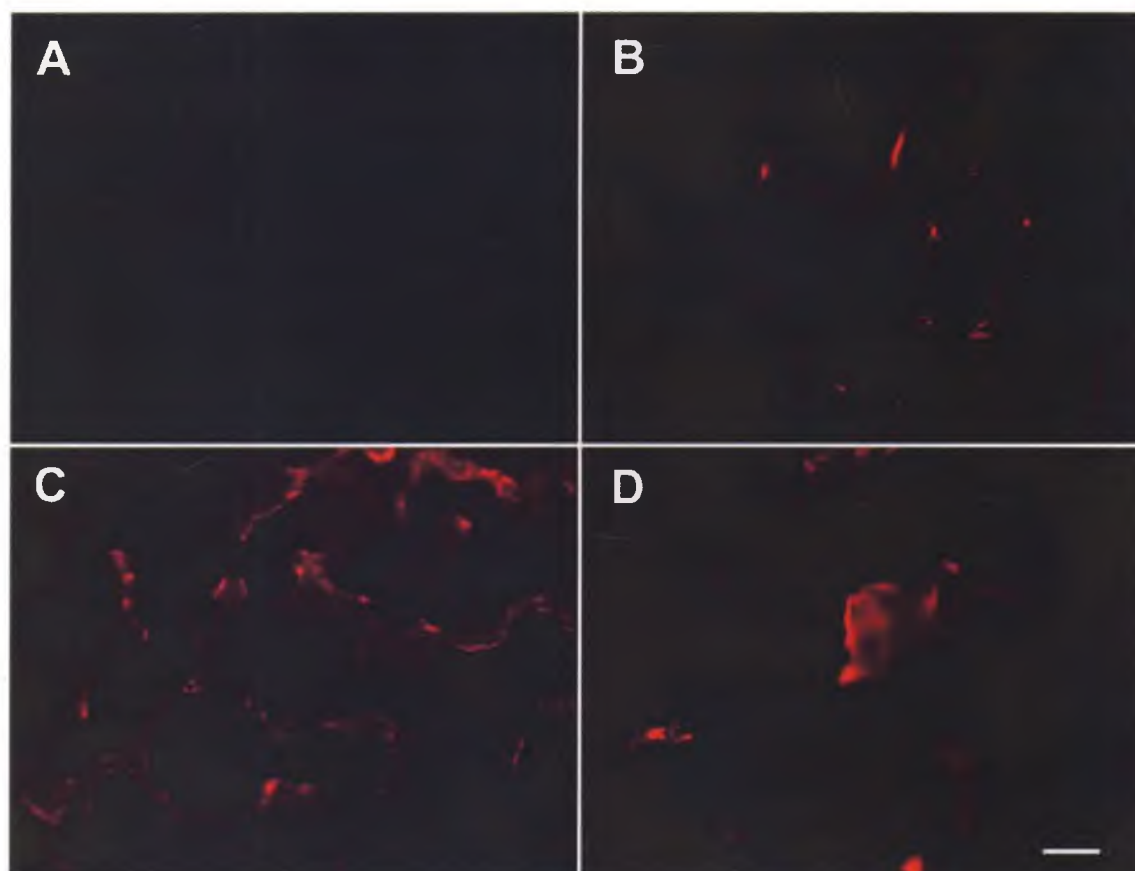


**Figure 23. Immunofluorescence results for various PCU-AA-FN scaffolds.** (A) PCU-AA; (B) 0.5 mg FN adsorbed on PCU-AA; (C) PCU-AA-FN (0.5 mg); (D) PCU-AA-FN (0.5 mg) after SDS leaching. The bar represents 100  $\mu\text{m}$ .

This supports the XPS survey scan findings, which showed that PCU-AA-FN (0.5 mg FN) had over three times greater nitrogen content than PCU-AA scaffolds with FN adsorption. Interestingly, when placed in a 2% (w/w) SDS solution, PCU-AA-FN scaffolds still stained positively for the antibody (Figure 23D), although the intensity of staining was reduced. SDS is an anionic detergent that denatures proteins by disrupting the non-covalent interactions between peptides, and was used to help extract any adsorbed FN on the scaffold surface. The FN would then re-form the H-bonds when placed in the PBS buffer, although perhaps in a slightly different conformation than the native one<sup>102</sup>. Since the primary antibody recognizes specific epitopes on the surface of

the FN molecule, changes in FN conformation will reduce the staining efficacy<sup>102</sup>. Hence, the reduction of fluorescence in these scaffolds was attributed to the loss of any adsorbed protein on the PCU-AA-FN scaffolds leaving behind only the immobilized FN (as seen in 3.5) as well as a reduction in antibody staining. Nonetheless, the principle that FN still exists on these PCU-AA-FN scaffolds after extensive SDS leaching is encouraging as it provides the insight that chemically immobilized FN will be able to withstand leaching conditions such as those introduced by a dynamic pulsatile flow bioreactor.

### **3.7 Preliminary Cell Culture Studies**

In order to evaluate vascular smooth muscle cell interactions with the various fabricated scaffolds, preliminary cell studies were conducted on PCU, PCU-AA, PCU-AA FN adsorbed and PCU-AA-FN scaffolds. For this preliminary cell work, scaffolds were seeded with  $7 \times 10^4$  cells/scaffold and cultured for a period of 4 days. The results are presented in Figure 24.

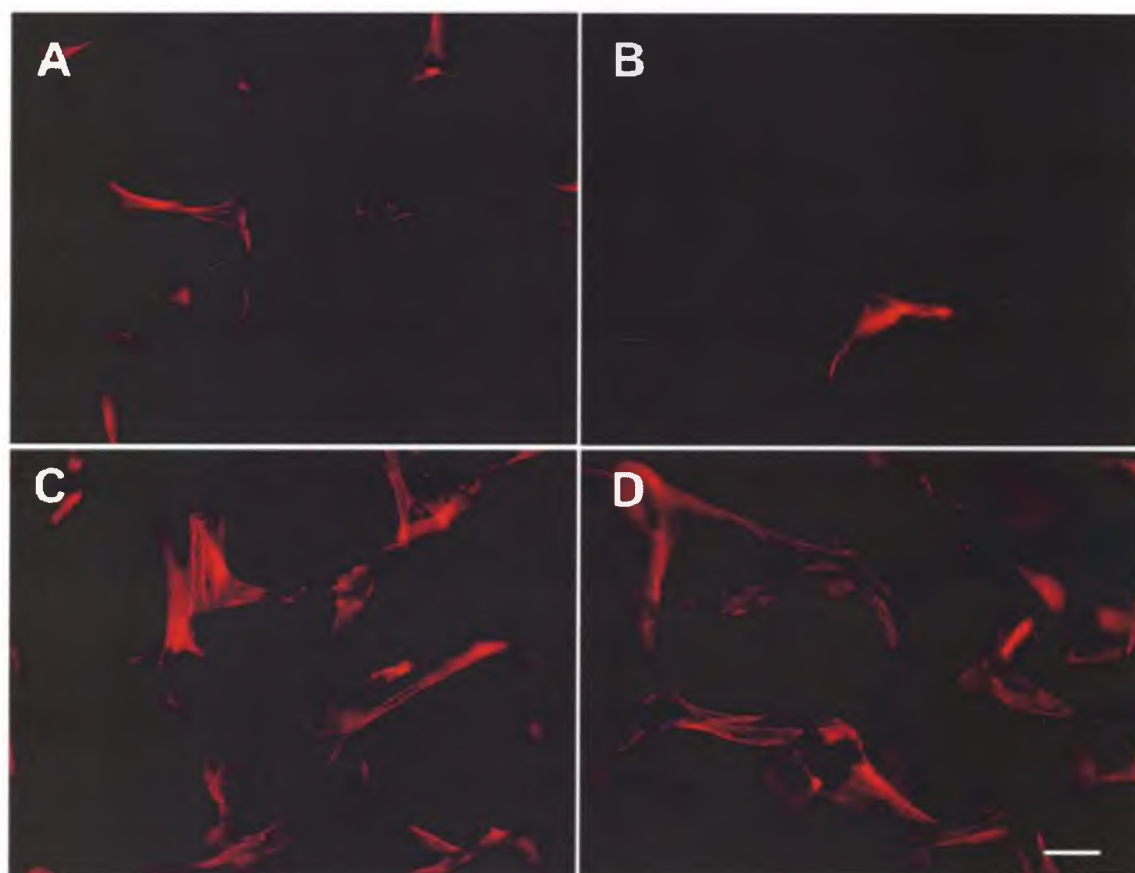


**Figure 24. Fluorescent microscope images of vascular smooth muscle cell behavior on (A) PCU; (B) PCU-AA; (C) PCU-AA FN adsorbed (0.5 mg FN); (D) PCU-AA-FN (0.5 mg FN) after 4 days of culture.**

In this image, phalloidin appears red from the Alexa Fluor® 568 stain. The PCU-AA surface appeared to be least favorable for cell growth. It is difficult to discriminate between C and D for the cell densities and culture time using a fluorescent microscope. The bar represents 100  $\mu\text{m}$ .

The phalloidin stain is useful in assessing cytoskeleton morphology, as vascular smooth muscle cells spread on favorable surfaces. As seen in Figure 24A, the unmodified PCU scaffolds had low cell numbers in comparison to those modified with FN (Figure 24C and D). It appeared that the PCU-AA scaffolds did not provide a good surface for cell attachment (Figure 24B). The surface of these scaffolds are covered in grafted polyacrylic acid chains (pKa 4.5), most of which are ionized at a neutral pH<sup>103</sup>. Furthermore, since polyacrylic acid is a known hydrogel, it has the ability to absorb significant amounts of water<sup>104</sup>. As a result, the surface of these scaffolds may have been unfavorable for cells to attach to in the presence of a boundary layer of water and was likely the cause of poor cell numbers on these scaffolds. On the other hand, FN modified scaffolds showed greater cell numbers since FN contains the cell adhesion motif, RGD. However, it was difficult to judge a difference in cell numbers between PCU-AA FN adsorbed and PCU-AA-FN scaffolds in 4 days cell culture using a fluorescent microscope which only shows cells on a single plane. Differences in cell growth between PCU-AA FN adsorbed and PCU-AA-FN scaffolds using a higher cell seeding density of  $1 \times 10^6$ /mL for 4 days culture period are presented in Figure 25. In order to provide a better depth perspective of cells on scaffolds, the images were taken using a confocal microscope.

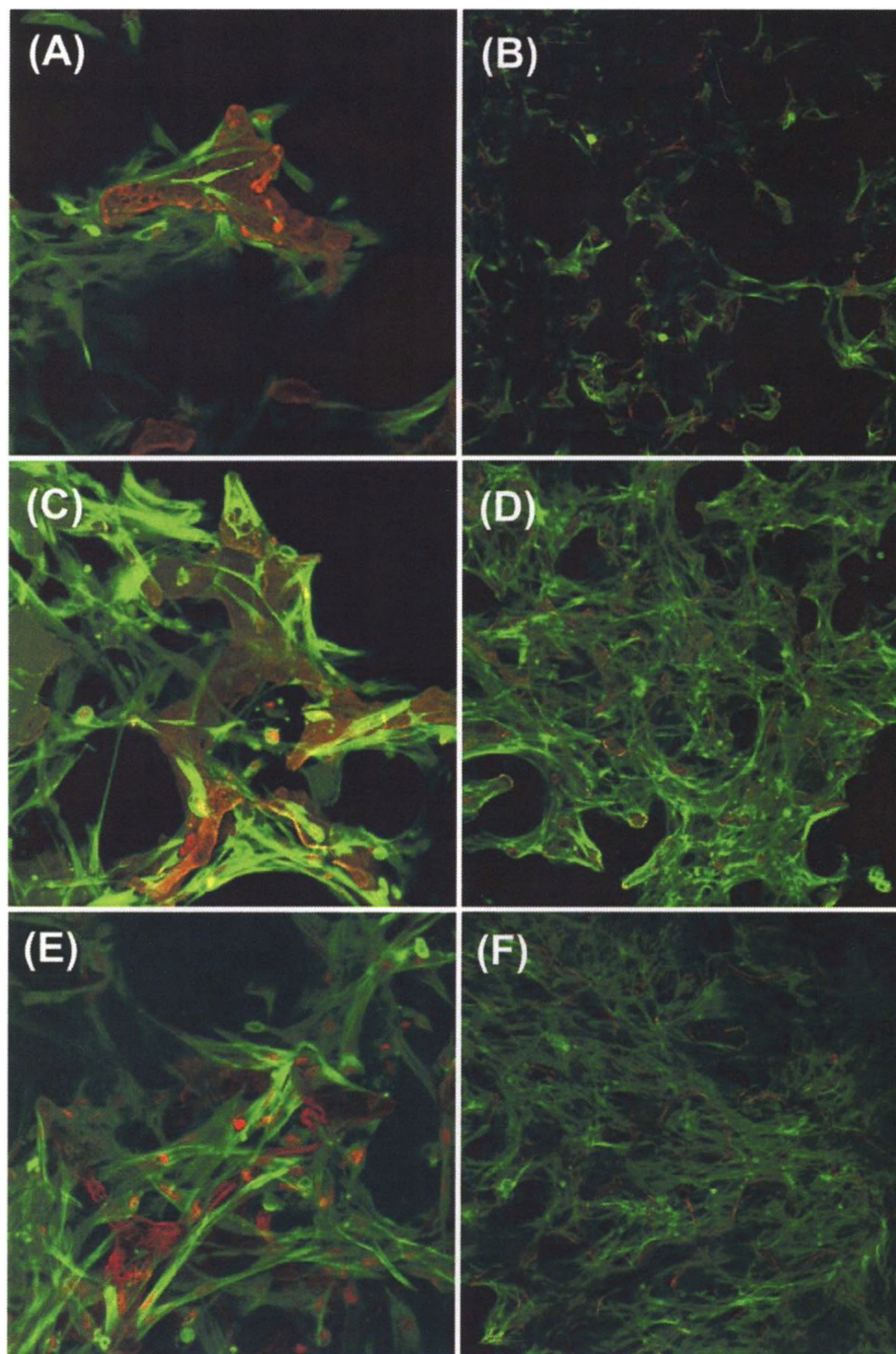


**Figure 25. Confocal microscope images of VSMC interaction with PCU-AA FN adsorbed (0.5 mg FN) (A-B); PCU-AA-FN (0.5 mg FN) (C-D); PCU-AA-FN (0.5 mg FN) exposed to 2% SDS (E-F), after 4 days culture. The cytoskeleton is stained in green and the struts of the scaffolds appear red.**

As seen in Figure 25, favorable VSMC interaction with PCU-AA FN adsorbed and PCU-AA-FN scaffolds was observed, and cells appeared to spread over the scaffolds. Although it appears that PCU-AA-FN scaffolds show more cell numbers compared to the FN adsorbed scaffolds qualitatively, quantification should be performed before we can draw any conclusions. PCU-AA-FN scaffolds that had been exposed to 2% SDS for 1 h (Figure 25E-F) also supported cell growth. This result was not unexpected, as the immunofluorescence results demonstrated that PCU-AA-FN scaffolds exposed to 2% SDS still showed the presence of FN (Figure 23D).

# CHAPTER 4

## 4 Conclusions

### 4.1 Summary

Numerous important goals were achieved in the described study. Three-dimensional, porous polyurethane scaffolds using a pressure differential SCPL method were fabricated. Acrylic acid was successfully grafted onto these scaffolds using a ceric ion initiator. The effect of AA concentration and time on the quantity of AA grafted onto the PCU scaffolds was studied, and as observed using SEM, overall 3D scaffold integrity and porosity was preserved for identified reaction conditions.

Several concentrations of fibronectin were conjugated onto these AA spacers, using EDC/NHS activation and stabilization steps. The end product was a biomimetic, 3D porous polyurethane scaffold. Scaffolds were characterized in order to validate the success of the chemistry. FT-IR, XPS survey and high resolution spectra, and immunofluorescence studies were conducted on the starting materials, intermediates, and final products.

Once it was established that FN was conjugated onto the 3D porous PCU scaffolds, human coronary artery vascular smooth muscle cells were seeded onto the scaffolds and

incubated for 4 days. Cytoskeletal staining revealed that PCU-AA FN adsorbed, PCU-AA-FN and PCU-AA-FN exposed to 2% SDS scaffolds supported VSMC growth.

The ultimate goal of vascular tissue engineering is to produce a functionally autologous and compliant vessel that can be implanted into the patient without the fear of host rejection and severe immune response. With continued persistence in research, this endeavor will be soon realized

## **4.2 Future Directions**

This study involved the chemical immobilization of fibronectin onto 3D porous, biostable polyurethane scaffolds and the subsequent evaluation of seeded vascular smooth muscle cell attachment and proliferation in 4 days of cell culturing.

As much of the presented cell work was preliminary, it would be necessary to count cell numbers and perform a statistical comparison of cell growth on the various scaffolds. Furthermore, cells could be cultured on the scaffolds for several weeks, and then the growing construct could be transferred into a perfusion bioreactor that would provide a constant flow of nutrient-rich serum as well as pulsatile mechanical stimulus. Specific proteins can be quantified using the Western Blotting technique, allowing one to study the effect of growth factors introduced into the serum (e.g. TGF- $\beta$ , retinoic acid) on protein expression in cells.

## References

1. Langer R, Vacanti JP. Tissue engineering. *Science* 1993;260(5110):920-6.
2. Rabkin E, Schoen FJ. Cardiovascular tissue engineering. *Cardiovascular Pathology* 2002;11(6):305-17.
3. Griffith LG, Naughton G. Tissue engineering-current challenges and expanding opportunities. *Science* 2002;295(5557):1009-14.
4. Griffith LG. Emerging design principles in biomaterials and scaffolds for tissue engineering. *Annals of New York Academy of Science* 2002;961:83-95.
5. Weir GC, Bonner-Weir S. Scientific and political impediments to successful islet transplantation. *Diabetes* 1997;46(8):1247-56.
6. Fan MY, Lum ZP, Fu XW, Levesque L, Tai IT, Sun AM. Reversal of diabetes in BB rats by transplantation of encapsulated pancreatic islets. *Diabetes* 1990;39(4):519-22.
7. Bilir BM, Guinette D, Karrer F, Kumpe DA, Krysl J, Stephens J, McGavran L, Ostrowska A, Durham J. Hepatocyte transplantation in acute liver failure. *Liver Transplantation* 2000;6(1):32-40.
8. El Oakley RM, Ooi OC, Bongso A, Yacoub MH. Myocyte transplantation for myocardial repair: a few good cells can mend a broken heart. *Annals of Thoracic Surgery* 2001;71(5):1724-33.
9. Van Meter CH, Jr., Claycomb WC, Delcarpio JB, Smith DM, deGruiter H, Smart F, Ochsner JL. Myoblast transplantation in the porcine model: a potential technique for myocardial repair. *Journal of Thoracic Cardiovascular Surgery* 1995;110(5):1442-8.
10. Roll S, Muller-Nordhorn J, Keil T, Scholz H, Eidt D, Greiner W, Willich SN. Dacron vs. PTFE as bypass materials in peripheral vascular surgery--systematic review and meta-analysis. *BMC Surgery* 2008;(8):8-22.
11. Kaushal S, Amiel GE, Guleserian KJ, Shapira OM, Perry T, Sutherland FW, Rabkin E, Moran AM, Schoen FJ, Atala A and others. Functional small-diameter neovessels created using endothelial progenitor cells expanded ex vivo. *Nature Medicine* 2001;7(9):1035-40.
12. Nasser BA, Ogawa K, Vacanti JP. Tissue engineering: an evolving 21st-century science to provide biologic replacement for reconstruction and transplantation. *Surgery* 2001;130(5):781-4.

13. Shieh SJ, Vacanti JP. State-of-the-art tissue engineering: from tissue engineering to organ building. *Surgery* 2005;137(1):1-7.
14. Rosamond W, Flegal K, Friday G, Furie K, Go A, Greenlund K, Haase N, Ho M, Howard V, Kissela B. Heart disease and stroke statistics - 2007 update: A Report from the American Heart Association Statistics Committee and Stroke Statistics Subcommittee. *Circulation* 2007;115(5): 69-171.
15. Manuel D, Leung M, Nguyen K, Tanuseputro P, Johansen H. Burden of cardiovascular disease in Canada. *Canadian Journal of Cardiology* 2003;19(9):997-1004.
16. Isenberg BC, Williams C, Tranquillo RT. Small-diameter artificial arteries engineered in vitro. *Circulation Research* 2006;98(1):25-35.
17. Campbell JH, Efendy JL, Campbell GR. Novel vascular graft grown within recipient's own peritoneal cavity. *Circulation Research* 1999;85(12):1173-8.
18. Ratcliffe A. Tissue engineering of vascular grafts. *Matrix Biology* 2000;19(4):353-7.
19. Hoenig MR, Campbell GR, Rolfe BE, Campbell JH. Tissue-engineered blood vessels: alternative to autologous grafts? *Arteriosclerosis Thrombosis and Vascular Biology* 2005;25(6):1128-34.
20. Dahl SL, Koh J, Prabhakar V, Niklason LE. Decellularized native and engineered arterial scaffolds for transplantation. *Cell Transplantation* 2003;12(6):659-66.
21. Gong Z, Niklason LE. Blood vessels engineered from human cells. *Trends Cardiovascular Medicine* 2006;16(5):153-6.
22. L'Heureux N, Paquet S, Labbe R, Germain L, Auger FA. A completely biological tissue-engineered human blood vessel. *FASEB Journal* 1998;12(1):47-56.
23. Patel A, Fine B, Sandig M, Mequanint K. Elastin biosynthesis: The missing link in tissue-engineered blood vessels. *Cardiovascular Research* 2006;71(1):40-9.
24. Weinberg CB, Bell E. A blood vessel model constructed from collagen and cultured vascular cells. *Science* 1986;231(4736):397-400.
25. Hirai J, Kanda K, Oka T, Matsuda T. Highly oriented, tubular hybrid vascular tissue for a low pressure circulatory system. *American Society for Artificial Organs* 1994;40(3):M383-8.
26. Niklason LE, Abbott W, Gao J, Klagges B, Hirschi KK, Ulubayram K, Conroy N, Jones R, Vasanawala A, Sanzgiri S and others. Morphologic and mechanical characteristics of engineered bovine arteries. *Journal of Vascular Surgery* 2001;33(3):628-38.

27. Berglund JD, Mohseni MM, Nerem RM, Sambanis A. A biological hybrid model for collagen-based tissue engineered vascular constructs. *Biomaterials* 2003;24(7):1241-54.
28. Manabe I, Nagai R. Regulation of smooth muscle phenotype. *Current Athlerosclerosis Reports* 2003;5(3):214-22.
29. Kielty C, Stephan S, Sherratt M, Williamson M, Shuttleworth C. Applying elastic fibre biology in vascular tissue engineering. *Philosophical Transactions of the Royal Society B: Biological Sciences* 2007;362(1484):1293-1312.
30. Owens GK, Kumar MS, Wamhoff BR. Molecular regulation of vascular smooth muscle cell differentiation in development and disease. *Physiology Reviews* 2004;84(3):767-801.
31. Hedin U, Thyberg J. Plasma fibronectin promotes modulation of arterial smooth-muscle cells from contractile to synthetic phenotype. *Differentiation* 1987;33(3):239-46.
32. Gupta V, Grande-Allen KJ. Effects of static and cyclic loading in regulating extracellular matrix synthesis by cardiovascular cells. *Cardiovascular Research* 2006;72(3):375-83.
33. Williams B. Mechanical influences on vascular smooth muscle cell function. *Journal of Hypertension* 1998;16(12 Pt 2):1921-9.
34. Kim BS, Nikolovski J, Bonadio J, Mooney DJ. Cyclic mechanical strain regulates the development of engineered smooth muscle tissue. *Nature Biotechnology* 1999;17(10):979-83.
35. Lu Q, Ganesan K, Simionescu DT, Vyavahare NR. Novel porous aortic elastin and collagen scaffolds for tissue engineering. *Biomaterials* 2004;25(22):5227-37.
36. Vats A, Tolley NS, Polak JM, Gough JE. Scaffolds and biomaterials for tissue engineering: a review of clinical applications. *Clinical Otolaryngology and Allied Sciences* 2003;28(3):165-72.
37. Neuenschwander S, Hoerstrup SP. Heart valve tissue engineering. *Transplant Immunology* 2004;12(3-4):359-65.
38. McFetridge PS, Daniel JW, Bodamyali T, Horrocks M, Chaudhuri JB. Preparation of porcine carotid arteries for vascular tissue engineering applications. *Journal of Biomedical Materials Research Part A* 2004;70(2):224-34.
39. Schaner PJ, Martin ND, Tulenko TN, Shapiro IM, Tarola NA, Leichter RF, Carabasi RA, Dimuzio PJ. Decellularized vein as a potential scaffold for vascular tissue engineering. *Journal of Vascular Surgery* 2004;40(1):146-53.

40. Mendelson K, Schoen FJ. Heart valve tissue engineering: concepts, approaches, progress, and challenges. *Annals of Biomedical Engineering* 2006;34(12):1799-819.
41. Badylak SF, Record R, Lindberg K, Hodde J, Park K. Small intestinal submucosa: a substrate for in vitro cell growth. *Journal of Biomaterial Science Polymer Edition* 1998;9(8):863-78.
42. Gunatillake PA, Adhikari R. Biodegradable synthetic polymers for tissue engineering. *European Cell Materials* 2003;(5):1-16.
43. Sodian R, Hoerstrup SP, Sperling JS, Daebritz SH, Martin DP, Schoen FJ, Vacanti JP, Mayer JE, Jr. Tissue engineering of heart valves: in vitro experiences. *The Annals of Thoracic Surgery* 2000;70(1):140-4.
44. Lamba NMK, Woodhouse KA, Cooper SL. *Polyurethanes in Biomedical Applications*: CRC Press; 1998.
45. Johansson S, Svineng G, Wennerberg K, Armulik A, Lohikangas L. Fibronectin-integrin interactions. *Frontiers in Bioscience* 1997;(2):126-46.
46. Pierschbacher MD, Ruoslahti E. Cell attachment activity of fibronectin can be duplicated by small synthetic fragments of the molecule. *Nature* 1984;309(5963):30-3.
47. Hedin U, Bottger BA, Forsberg E, Johansson S, Thyberg J. Diverse effects of fibronectin and laminin on phenotypic properties of cultured arterial smooth muscle cells. *Journal of Cell Biology* 1988;107(1):307-19.
48. Hersel U, Dahmen C, Kessler H. RGD modified polymers: biomaterials for stimulated cell adhesion and beyond. *Biomaterials* 2003;24(24):4385-415.
49. Merz Kirch C, Davies N, Zilla P. Engineering of vascular ingrowth matrices: are protein domains an alternative to peptides? *The Anatomical Record* 2001;263(4):379-87.
50. Heilshorn SC, DiZio KA, Welsh ER, Tirrell DA. Endothelial cell adhesion to the fibronectin CS5 domain in artificial extracellular matrix proteins. *Biomaterials* 2003;24(23):4245-52.
51. Benoit DS, Anseth KS. The effect on osteoblast function of colocalized RGD and PHSRN epitopes on PEG surfaces. *Biomaterials* 2005;26(25):5209-20.
52. Feng Y, Mrksich M. The synergy peptide PHSRN and the adhesion peptide RGD mediate cell adhesion through a common mechanism. *Biochemistry* 2004;43(50):15811-21.

53. Mooney DJ, Baldwin DF, Suh NP, Vacanti JP, Langer R. Novel approach to fabricate porous sponges of poly (D, L-lactic-co-glycolic acid) without the use of organic solvents. *Biomaterials* 1996;17(14):1417-22.
54. Mikos AG, Bao Y, Cima LG, Ingber DE, Vacanti JP, Langer R. Preparation of poly (glycolic acid) bonded fiber structures for cell attachment and transplantation. *Journal of Biomedical Materials Research* 1993;27(2):183-89.
55. Whang K, Thomas C, Healy K, Nuber G. A novel method to fabricate bioabsorbable scaffolds. *Polymer* 1995;(36):837-842.
56. Mikos AG, Thorsen AJ, Czerwonka LA, Bao Y, Langer R, Winslow DN, Vacanti JP. Preparation and characterization of poly (L-lactic acid) foams. *Polymer* 1994;35(5):1068-1077.
57. Mikos AG, Temenoff JS. Formation of highly porous biodegradable scaffolds for tissue engineering. *Electronic Journal of Biotechnology* 2000;(3):23-24.
58. Mikos AG, Temenoff, J., Lu, L., Teßmar, Jörg. Synthetic Bioresorbable Polymer Scaffolds. In: Ratner BD, Hoffman, A., Schoen, F., Lemons, J.. *Biomaterials science: an introduction to materials in medicine*; San Diego: Academic press; 1997. p 735.
59. Lee J, Cuddihy MJ, Kotov NA. Three-dimensional cell culture matrices: state of the art. *Tissue Engineering Part B Reviews* 2008;14(1):61-86.
60. Yeong WY, Chua CK, Leong KF, Chandrasekaran M. Rapid prototyping in tissue engineering: challenges and potential. *Trends in Biotechnology* 2004;22(12):643-652.
61. Hutmacher DW. Scaffold design and fabrication technologies for engineering tissues-state of the art and future perspectives. *Journal of Biomaterials Science, Polymer Edition* 2001;12(1):107-24.
62. Barnes CP, Sell SA, Boland ED, Simpson DG, Bowlin GL. Nanofiber technology: Designing the next generation of tissue engineering scaffolds. *Advanced Drug Delivery Reviews* 2007;59(14):1413-33.
63. Lannutti J, Reneker D, Ma T, Tomasko D, Farson D. Electrospinning for tissue engineering scaffolds. *Materials Science and Engineering* 2007;27(3):504-09.
64. Jaumotte-Thelen S, Dozot-Dupont I, Marchand-Brynaert J. Covalent grafting of fibronectin and asialofetuin at surface of poly (ethylene terephthalate) track-etched membranes improves adhesion but not differentiation of rat hepatocytes. *Journal of Biomedical Materials Research* 1996;(32):569-82.

65. Zhang Y, Chai C, Jiang XS, Teoh SH, Leong KW. Fibronectin immobilized by covalent conjugation or physical adsorption shows different bioactivity on aminated-PET. *Materials Science and Engineering: C* 2007;27(2):213-19.
66. Nagai M, Hayakawa T, Makimura M, Yoshinari M. Fibronectin Immobilization using Water-soluble Carbodiimide on Poly-L-lactic Acid for Enhancing Initial Fibroblast Attachment. *Journal of Biomaterials Applications* 2006;21(1):33-47.
67. Vo lcker N, Klee D, Hocker H, Langefeld S. Functionalization of silicone rubber for the covalent immobilization of fibronectin. *Journal of Materials Science: Materials in Medicine* 2001;12(2):111-19.
68. Ko IK, Iwata H. An approach to constructing three-dimensional tissue. *Annals of the New York Academy of Science* 2001;(944):443-55.
69. Hayakawa T, Yoshinari M, Nemoto K. Direct attachment of fibronectin to tresyl chloride-activated titanium. *Journal of Biomedical Material Research Part A* 2003;67(2):684-8.
70. Hayakawa T, Nagai M, Yoshinari M, Makimura M, Nemoto K. Cell-adhesive Protein Immobilization Using Tresyl Chloride-activation Technique for the Enhancement of Initial Cell Attachment. *Journal of Oral Tissue Engineering* 2004;2(1):14-24.
71. Webb K, Caldwell K, Tresco P. A novel surfactant-based immobilization method for varying substrate-bound fibronectin. *Journal of Biomedical Materials Research* 2001;54(4):509-518.
72. Zhu Y, Leong M, Ong W, Chan-Park M, Chian K. Esophageal epithelium regeneration on fibronectin grafted poly (l-lactide-co-caprolactone)(PLLC) nanofiber scaffold. *Biomaterials* 2007;28(5):861-68.
73. Gauvreau V, Chevallier P, Vallieres K, Petitclerc E, Gaudreault RC, Laroche G. Engineering surfaces for bioconjugation: developing strategies and quantifying the extent of the reactions. *Bioconjugate Chemistry* 2004;15(5):1146-56.
74. Vallieres K, Chevallier P, Sarra-Bournet C, Turgeon S, Laroche G. AFM imaging of immobilized fibronectin: does the surface conjugation scheme affect the protein orientation/conformation? *Langmuir* 2007;23(19):9745-51.
75. Sakiyama-Elbert S, Hubbell J. Functional Biomaterials: Design of Novel Biomaterials. *Annual Reviews in Materials Research* 2001;31(1):183-201.
76. Lu Y, Mapili G, Suhali G, Chen S, Roy K. A digital micro-mirror device-based system for the microfabrication of complex, spatially patterned tissue engineering scaffolds. *Journal of Biomedical Materials Research Part A* 2006;77(2):396-405.

77. Feng Q, Chai C, Jiang X, Leong K, Mao H. Expansion of engrafting human **hematopoietic stem/progenitor** cells in three-dimensional scaffolds with surface-immobilized **fibronectin**. *Cytokines* 2006;(18):781-791.
78. Bramfeldt H, Vermette P. Enhanced smooth muscle cell adhesion and proliferation on protein-modified polycaprolactone-based copolymers. *Journal of Biomedical Materials Research Part A* (In Press).
79. Gunatillake PA, Adhikari R. Biodegradable synthetic polymers for tissue engineering. *European Cells and Materials* 2003;5(1):1-16.
80. Shin H, Jo S, Mikos AG. Biomimetic materials for tissue engineering. *Biomaterials* 2003;24(24):4353-64.
81. Feng XD, Sun YH, Qiu KY. Reactive site and mechanism of graft copolymerization onto poly (ether urethane) with ceric ion as initiator. *Macromolecules* 1985;18(11):2105-09.
82. Uchida E, Uyama Y, Ikada Y. Sorption of low-molecular-weight anions into thin polycation layers grafted onto a film. *Langmuir* 1993;9(4):1121-24.
83. Walker J. The bicinchoninic acid (BCA) assay for protein quantitation. *Methods in Molecular Biology* 1994;32:5-8.
84. Wan AC, Mao HQ, Wang S, Phua SH, Lee GP, Pan J, Lu S, Wang J, Leong KW. Poly(phosphoester) ionomers as tissue-engineering scaffolds. *Journal of Biomedical Materials Research Part B* 2004;70(1):91-102.
85. Hermanson GT. *Bioconjugate Techniques*: Academic Press; Rockford, USA, 2008.
86. Mattson G, Conklin E, Desai S, Nielander G, Savage MD, Morgensen S. A practical approach to crosslinking. *Molecular Biology Reports* 1993;17(3):167-83.
87. Pitt W, Spiegelberg S, Cooper S. Adsorption of fibronectin to polyurethane surfaces: Fourier transform infrared spectroscopic studies. *Proteins at interfaces: physiochemical and biochemical studies*. American Chemical Society, Washington, DC 1987:324-38.
88. Giroux T, Cooper S. FTIR/ATR studies of human fibronectin adsorption onto plasma derivatized polystyrene. *Journal of colloid and interface science* 1990;139(2):351-62.
89. Koteliansky VE, Glukhova MA, Bejanian MV, Smirnov VN, Filimonov VV, Zalite OM, Venyaminov S. A study of the structure of fibronectin. *European Journal of Biochemistry* 1981;119(3):619-24.

90. Chansook N, Kiatkamjornwong S. Ce (IV)-Initiated Graft Polymerization of Acrylic Acid onto Poly (ethylene terephthalate) Fiber. *Journal of Applied Polymer Science* 2003;89(7):1952-58.
91. Gupta KC, Khandekar K. Graft copolymerization of acrylamide-methylacrylate comonomers onto cellulose using ceric ammonium nitrate. *Journal of Applied Polymer Science* 2002;86(10):2631-42.
92. Tooney NM. Solution and surface effects on plasma fibronectin structure. *The Journal of Cell Biology* 1983;97(6):1686-92.
93. Barbani N, Lazzeri L, Cristallini C, Cascone MG, Polacco G, Pizzirani G. Bioartificial materials based on blends of collagen and poly (acrylic acid). *Journal of Applied Polymer Science* 1999;72(7):971-76.
94. Hollmann O, Czeslik C. Characterization of a planar poly (acrylic acid) brush as a materials coating for controlled protein immobilization. *Langmuir* 2006;22(7):3300-05.
95. Galtayries A, Warocquier-Clerout R, Nagel M, Marcus P. Fibronectin adsorption on Fe-Cr alloy studied by XPS. *Surface and Interface Analysis* 2006;38(4):186-190.
96. Zhu Y, Chian KS, Chan-Park MB, Mhaisalkar PS, Ratner BD. Protein bonding on biodegradable poly(L-lactide-co-caprolactone) membrane for esophageal tissue engineering. *Biomaterials* 2006;27(1):68-78.
97. McMillan R, Meeks B, Bensebaa F, Deslandes Y, Sheardown H. Cell adhesion peptide modification of gold-coated polyurethanes for vascular endothelial cell adhesion. *Journal of Biomedical Materials Research* 2001;54(2):272-83.
98. Xiao SJ, Textor M, Spencer ND, Wieland M, Keller B, Sigrist H. Immobilization of the cell-adhesive peptide Arg-Gly-Asp-Cys (RGDC) on titanium surfaces by covalent chemical attachment. *Journal of Materials Science: Materials in Medicine* 1997;8(12):867-72.
99. Tang YW, Labow RS, Revenko I, Santerre JP. Influence of surface morphology and chemistry on the enzyme catalyzed biodegradation of polycarbonate-urethanes. *Journal of Biomaterial Science Polymer Edition* 2002;13(4):463-83.
100. Volcker N, Klee D, Hocker H, Langefeld S. Functionalization of silicone rubber for the covalent immobilization of fibronectin. *Journal of Materials Science: Materials in Medicine* 2001;12(2):111-9.
101. Guan J, Gao C, Feng L, Shen J. Preparation of functional poly (ether-urethane) for immobilization of human living cells 1. Surface graft polymerization of poly (ether-urethane) with 2-(dimethylamino) ethyl methacrylate and quaternization of grafted membrane. *European Polymer Journal* 2000;36(12):2707-13.

102. Brändén C, Tooze J. Introduction to protein structure: Routledge; New York, USA, 1999.
103. Groves M. Pharmaceutical Biotechnology: CRC Press; London, UK, 2006.
104. Elliott J, Macdonald M, Nie J, Bowman C. Structure and swelling of poly (acrylic acid) hydrogels: effect of pH, ionic strength, and dilution on the crosslinked polymer structure. *Polymer* 2004;45(5):1503-10.

## Appendix A: Tabulated XPS Survey Scan Data

Sample	Carbon	Nitrogen	Oxygen	Sulfur
PCU	74.5	3.1	22.4	0.0
PCU	77.2	3.3	19.2	0.0
PCU	75.0	3.8	21.3	0.0
PCU-AA (1hr AA)	76.0	0.0	24.0	0.0
PCU-AA (1hr AA)	77.1	1.1	21.8	0.0
PCU-AA (1hr AA)	74.9	0.8	24.2	0.0
PCU-AA-NHS	69.3	12.4	18.3	0.0
PCU-AA-NHS	68.1	8.1	23.7	0.0
PCU-AA-NHS	69.0	10.6	20.4	0.0
PCU-AA-FN (1hr AA, 0.1mg FN)	66.6	5.8	28.0	0.1
PCU-AA-FN (1hr AA, 0.1mg FN)	68.7	3.4	27.9	0.0
PCU-AA-FN (1hr AA, 0.1mg FN)	68.8	4.4	26.1	0.0
PCU-AA-FN (1hr AA, 0.2mg FN)	67.5	8.4	23.9	0.3
PCU-AA-FN (1hr AA, 0.2mg FN)	73.8	6.8	19.4	0.0
PCU-AA-FN (1hr AA, 0.2mg FN)	65.9	6.3	25.8	0.7
PCU-AA, FN ads (1hr AA, 0.5mg FN)	72.5	3.3	24.2	0.3
PCU-AA, FN ads (1hr AA, 0.5mg FN)	73.1	2.2	24.8	0.0
PCU-AA, FN ads (1hr AA, 0.5mg FN)	72.8	4.3	22.5	0.4
PCU-AA (6hr AA)	73.7	0.0	26.4	0.0
PCU-AA-FN (6hr AA, 0.2mg FN)	65.2	10.4	24.0	0.5
PCU-AA-FN (6hr AA, 0.5mg FN)	65.8	13.1	20.6	0.3
PCU-AA, FN ads (6hr AA, 0.5mg FN)	66.7	11.7	21.3	0.2
PCU-AA-FN (0.5mg FN, 1hr conjugation)	69.2	10.4	20.2	0.3
PCU-AA-FN (0.5mg FN, 1hr conjugation)	71.4	8.1	20.5	0.0
PCU-AA-FN (0.5mg FN, 1hr conjugation)	67.9	11.9	19.8	0.3
PCU-AA-FN (0.5mg FN, 6hr conjugation)	69.9	10.1	19.7	0.3
PCU-AA-FN (0.5mg FN, 6hr conjugation)	68.0	12.3	19.5	0.3
PCU-AA-FN (0.5mg FN, 6hr conjugation)	69.6	10.9	19.3	0.2
PCU-AA-FN (0.5mg FN, 12hr conjugation)	69.5	12.6	17.5	0.3
PCU-AA-FN (0.5mg FN, 12hr conjugation)	70.1	10.9	18.4	0.5
PCU-AA-FN (0.5mg FN, 12hr conjugation)	69.3	11.5	18.6	0.5
PCU-AA-FN (0.5mg FN, 24hr conjugation)	66.7	11.2	21.6	0.4
PCU-AA-FN (0.5mg FN, 24hr conjugation)	68.3	10.9	20.0	0.8
PCU-AA-FN (0.5mg FN, 24hr conjugation)	66.6	12.4	20.5	0.6